REPORT DOCUMENTATION PAGE

AFRL-SR-AR-TR-03-

02168

88

1. AGENCY USE ONLY *(Leave blank)*	2. REPORT DATE	3. REPORT TYPE AND DATES COVERED
		01 May 2000 - 30 Apr 2003 Final Report

4. TITLE AND SUBTITLE
Laser and Radio Frequency Air Plasma Sources

5. FUNDING NUMBERS
61102F
2301/EX

6. AUTHOR(S)
Professor Scharer

7. PERFORMING ORGANIZATION NAME(S) AND ADDRESS(ES)
UNIVERSITY OF WISCONSIN
750 UNIVERSITY AVENUE
MADISON WI 53706-1490

8. PERFORMING ORGANIZATION REPORT NUMBER

9. SPONSORING/MONITORING AGENCY NAME(S) AND ADDRESS(ES)
AFOSR/NE
4015 WILSON BLVD
SUITE 713
ARLINGTON VA 22203

10. SPONSORING/MONITORING AGENCY REPORT NUMBER
F49620-00-1-0181

11. SUPPLEMENTARY NOTES

12a. DISTRIBUTION AVAILABILITY STATEMENT
APPROVED FOR PUBLIC RELEASE, DISTRIBUTION UNLIMITED

12b. DISTRIBUTION CODE

13. ABSTRACT *(Maximum 200 words)*

We have made substantial progress in producing laser initiated seeded organic gas plasmas in air with densities of 1x10 13/cc of 500 cc volumes with low temperatures of 0.3 eV. We have measured plasma density decay rates and been successful in radiofrequency sustainment of the laser-produced plasmas with reduced power levels compared to radiofrequency ionization alone. The laser-produced plasmas provide a load for the radiofrequency coupled power through the antenna that greatly enhances power coupling efficiency to the plasma. It greatly reduces the reflected power from the antenna-plasma load and suppresses transient processes that reduce the available radiofrequency power that can be coupled tot he plasma.

14. SUBJECT TERMS			15. NUMBER OF PAGES
			16. PRICE CODE
17. SECURITY CLASSIFICATION OF REPORT	18. SECURITY CLASSIFICATION OF THIS PAGE	19. SECURITY CLASSIFICATION OF ABSTRACT	20. LIMITATION OF ABSTRACT
UNCLASSIFIED	UNCLASSIFIED	UNCLASSIFIED	UL

Final Progress Report
Laser and Radiofrequency Air Plasma Sources
AFOSR Grant No. F49620-00-1-0181
May 1, 2000 through April 30, 2003

J. E. Scharer, Principal Investigator
Department of Electrical and Computer Engineering
University of Wisconsin, Madison, WI 53706

Abstract

High density ($4x10^{13}$-10^{12}/cc), large volume (500-3000 cc), high-pressure (10-760 Torr) laser initiated, radiofrequency (RF) sustained plasmas were produced in nitrogen, argon and air. We have produced $4x10^{13}$/cc, low temperature (Te<0.3 eV), 500 cc seeded organic gas plasmas with our pulsed 193 nm laser source. Recombination rates and evidence for delayed ionization due to super-excited states were found. When 15 mTorr of the seed gas is mixed with air, nitrogen, argon or helium at 760 Torr, the laser-produced density is in the range of 1-3x 10^{13}/cc and plasma decay and 2 and 3-body recombination rates have been measured. Research on seeded, high-pressure air plasmas has been carried out using new, advanced, state-of-the-art research equipment made possible by an AFOSR equipment grant (Grant No. F49620-00-1-0032) with substantial matching funds from the University of Wisconsin. Improvements in the radiofrequency antenna power coupling and capacitive matching system has allowed us to obtain 10 cm diameter line-average plasma densities of $9x10^{13}$- $5x10^{12}$/cc in Argon/N_2/Air mixes in the 10-250 Torr range at moderate radio-frequency (RF) power levels of 2 kW. We have also carried out short (6 ms) and long pulse ($\geq$ 10 sec) RF sustainment of the 193 nm laser-initiated, seeded plasmas. We have sustained laser seed gas initiated, large volume (2500 cc), and high average density > 5 x 10^{12}/cc argon plasmas at gas pressures from 10- 700 Torr, with low RF power densities of 0.05-0.6 W/cc. The use of the laser produced TMAE seed plasma to provide a load for radiofrequency antenna matching provides a significant reduction in sustainment power compared to high-pressure radiofrequency plasma creation alone. TMAE is compatible with air over long times and that it is quite viable for efficient laser ionization in air for 5-10 minutes after introduction Spectroscopic measurements have been made to determine the electron excitation temperature and ion species concentration from the spectral content of the plasmas. We have also examined swirl gas flow that produces a more uniform axial temperature profile. This leads to an improvement in plasma density and volume and reduction in the effective recombination rate as compared to the static case. We have also carried out initial experiments on magnetized RF plasma sources to examine enhanced RF wave penetration and skin depth effects in high-density collisional plasmas. We also developed for the first time, to our knowledge, a new method of interferometry analysis for highly collisional plasmas where the plasma density, effective collisionality and recombination rates during the plasma decay can be obtained. We have applied this to our 105 GHz mm wave interferometer diagnostic measurements with excellent results. We are also making contributions and serving as Chapter Master for material on High Frequency Air Plasma Production and contributing to the Diagnostic Chapter for a new book on Non-Equilibrium Air Plasmas to be published by the Institute of Physics. Graduate students participating in the research, five reviewed journal publications, an invited paper and conference publications presented are also described.

Table of Contents

I. Introduction

Substantial progress has been made in producing seeded high-pressure air plasmas by both laser and radiofrequency (RF) methods. The use of a pulsed ultraviolet (UV) excimer laser to produce large volume (500 cc) seed plasmas for enhanced loading and sustainment by lower power radiofrequency antenna coupling is the major focus of the research. We have also achieved long pulse (> 10 sec) RF sustainment of laser-initiated, seeded air plasmas. It should be noted that this research has produced large volume plasmas of 500-8500 cm^3 at high densities in the 10^{13}-$10^{12}/cm^3$ range. Two new RF sources with power ranges of 1-25 kW have been installed and used for high density air plasma production. A new, efficient capacitive matching network and an antenna system have been installed to minimize ohmic circuit losses. We have also used a 105 GHz mm wave interferometer and developed a model and code to obtain accurate plasma density measurements in the presence of high collisionality. Additional diagnostics include a multi-channel spectrometer for electron plasma temperature measurements, a fiber optic probe for measurements of fast electron emission, and fast response Langmuir and wave magnetic field B-dot probes.

We feel that an important method for obtaining high pressure atmospheric plasmas can be achieved by injecting seeded atomic gases and preionization of low ionization energy seed organic gas followed by sustainment of the plasma at lower RF powers. In addition, we also anticipate, based on our preliminary experiments, that high-speed gas flow improves the plasma density and volume by an order of magnitude in comparison to that in the static case. Axial plasma flow reduces radial diffusion of plasma to the wall leading to substantial loss of RF power in heating the plasma chamber. In addition, the gas flow leads to a more uniform axial temperature profile. Furthermore, reducing negative ion formation in air to reduce the energy budget and utilizing metastable states to enhance ionization is also attractive. By increasing the neutral gas temperature to 2000 ^0K, a reduction in the oxygen negative ion formation can be accomplished and higher electron density air plasmas can be obtained. These plasmas are of considerable interest in plasma materials processing, reducing pollutants in hazardous industrial gases, biological decontamination, radar reflection, shielding or cross-section modification and reduction of supersonic drag. It should also be noted that at altitudes of 30,000 to 100,000 feet where aircraft can operate the ambient air pressures are in the 270 to

24 Torr range and the constituents are comparable to those at sea level. Thus producing large volume, high density air plasmas at these pressures with minimum power requirements is of interest and the lower air pressures at altitudes will allow this to be done at lower power densities by seeded gas injection in air.

The research progress, journal, invited papers and conference publications, personnel and degrees completed are included in this report. The following research areas are described in detail in the report. These are:

1. Laser initiation and recombination rate measurements of high density (10^{13} -10^{14}/cc), large volume (500 cc) organic gas seeded air plasmas at up to 760 Torr pressures for nitrogen, air, oxygen, argon and helium.
2. Long pulse (>10 Sec), large volume (2500 cc) RF sustainment of laser-initiated, organic gas seeded plasmas.
3. Steady-state creation of large volume (3500 cc), seeded air plasmas at high gas pressures and the gas flow enhancement of plasma characteristics.
4. Radiofrequency creation and measurement of enhanced wave penetration in high density plasmas ($10^{12\text{-}13}$/ cc) in a magnetic field.
5. Development of optical diagnostic of air, nitrogen, oxygen, and argon laser and radiofrequency produced plasmas and mm wave interferometric measurement of density and recombination rates for high collisionality at high gas pressures.
6. We are also contributing a discussion of new mm wave diagnostics to the Diagnostics Chapter and serving as Chapter Master of the Section on High Frequency Creation of Plasmas to a new book entitled Non-Equilibrium Air Plasmas to be published by the Institute of Physics.

II. Research Progress Highlights

The following are the highlights of our research:

- Laser created, accurately diagnosed, high density (10^{13}/cc), large volume (500 cc), low temperature (T_e=0.3 eV) organic gas plasmas as a seed for nitrogen at up to 760 Torr.

- First observation and publication of super excited, laser-produced seed gas states which cause delayed ionization and increased lifetime in nitrogen at densities ~$10^{13\text{-}12}$/cm^3 and pressures at up to 760 Torr.

  [G. Ding, J.E. Scharer, K. Kelly," Physics of Plasmas, Vol. 8, No. 1, 334 (2001)]

- Measurements of high density (10^{13}/cc), laser created organic seed plasmas and recombination rates in air, nitrogen, oxygen, argon and helium at up to 760 Torr. ***[Kamran Akhtar, J. Scharer, S. Tysk, and M. Denning, To be published in the proceedings of 15th topical conference on Radio Frequency Power in Plasmas, Jackson Lake Lodge, Grand Teton National Park, Moran, Wyoming, May19-21, 2003, AIP].***

- Obtained and published results of long pulse (4 ms), large volume (500 cc) 2.2 kW radiofrequency sustainment of laser-initiated seed plasmas ($8x10^{12}$/cm^3) at 150 Torr pressures which is twice that of radiofrequency creation alone.[3] [***K. L. Kelly, J.E. Scharer, E.S. Paller, and G. Ding, "Laser Ionization and Radiofrequency Sustainment of High-Pressure Seeded Plasmas", Jour. of Applied Physics, Vol. 92, No. 2, 698-709, 2002.]***

- We have further improved the experimental facility to obtain large volume plasmas (2500 cc) at high density (1×10^{12}-9×10^{13} /cc) in the pressure range 100 - 760 Torr at 2-5 kW RF power levels.

- We have investigated and confirmed that gas flow improves the plasma density and volume by at least an order of magnitude. The strong axial temperature gradient present during static discharges causes the plasma to be contracted under the antenna. We have seen that gas flow substantially reduces the axial temperature gradient and produces an extended plasma volume (5000-6000 cc) of high density (~ 10^{13} cc) and lower effective collision frequency (~10^{10}/s) at atmospheric pressure.

- Developed millimeter wave interferometry for high-pressure collisional discharges.

  [K. Akhtar, J. Scharer, S. Tysk, and E. Kho, Rev. Sci. Instrum., 74, 996 (2003)].

- Employed optical spectrometer probes and millimeter wave interferometer for diagnostic measurements of seeded air plasmas. We have also acquired fast scopes (4 Gs/s) and high power (10-25 kW) pulsable radiofrequency generators which allows measurement of high plasma density in the presence of high collisionality at high gas

pressures. We are contributing a discussion of new mm wave high pressure plasma diagnostics to the Diagnostics Chapter of a book on Non-Equilibrium Air Plasmas. We are also serving as Chapter Master of and contributing to the Section on High Frequency Creation of Plasmas to a book entitled Non-Equilibrium Air Plasmas to be published by the Institute of Physics.

- Published five reviewed journal articles, one invited paper, twenty-five conference papers, and graduated four students during the period 5/00-4/03.

III. Laser Produced TMAE Plasma seeded in high-pressure air constituent gases

A. Laser plasma experimental system

A schematic experimental arrangement is illustrated in Fig.1. Two plasma chambers, a 150 cm long by 5 cm diameter and a 50 cm long by 15.2 cm diameter are pumped to a base pressure of 5×10^{-7} Torr by a turbo molecular pump. A Suprasil window which is transparent down to 180 nm wavelengths is mounted on the laser entrance end of the vacuum chamber. Gas mass flow controllers along with a swirl gas injection system are also located at this end as shown in Fig. 1. On the opposite side of the chamber, a Langmuir probes (LP), one with a heater for ultra-clean probe surfaces and the second as a dummy probe for differential current measurements that suppress the laser and plasma transient noise yet have high frequency, fast 5 ns plasma response times is inserted through a feed-through to the vacuum chamber.

A Lumonics PM842 excimer laser runs in an ArF mode and produces 193 nm wavelength radiation. The half-width of the laser pulse is 20 ns. The shape of laser output cross section initially is a rectangle of 2.8 cm × 1.2 cm. It can be changed simply by a two-lens system. The laser output cross-section of 2.8×1.2 cm^2 can be increased to 2.8×2.8 cm^2 using a lens system of fused silica cylindrical plano-convex and plano-concave lenses in order to increase the plasma filling fraction of the vacuum chamber. The laser beam is quite uniform over the cross-section, $\Delta I/I\sim10\%$ as measured by a pinhole aperture photodiode. A calorimeter is also used to accurately measure the intensity of the laser beam. For LP measurement, the laser first passes through a beam splitter and part of the beam is used to trigger the boxcar

averager and LP driver. The plasma diagnostics also includes millimeter wave interferometry developed for high pressure plasmas along with plasma emission spectroscopy.

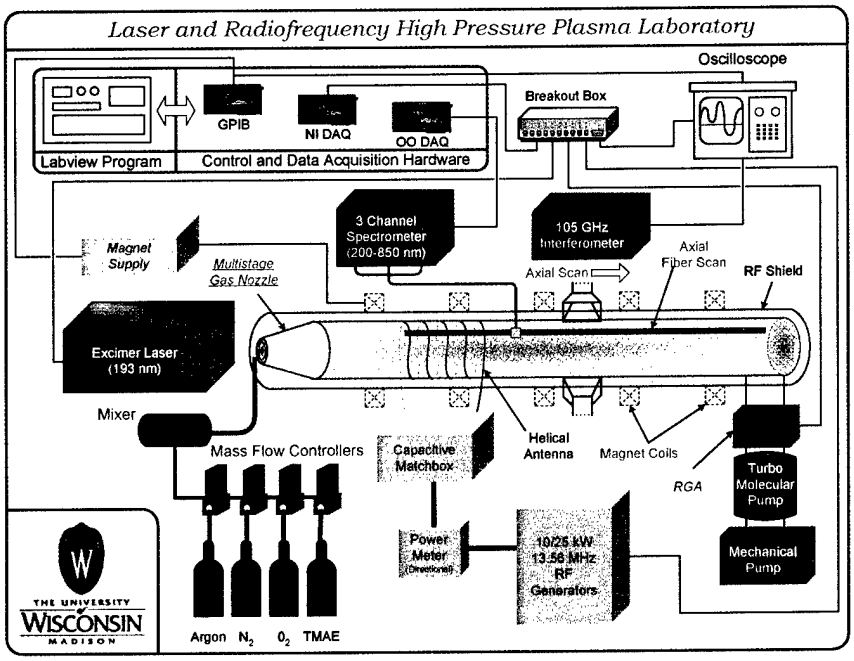

Fig. 1. Experimental configuration for laser-initiation and radio-frequency sustainment plasma source.

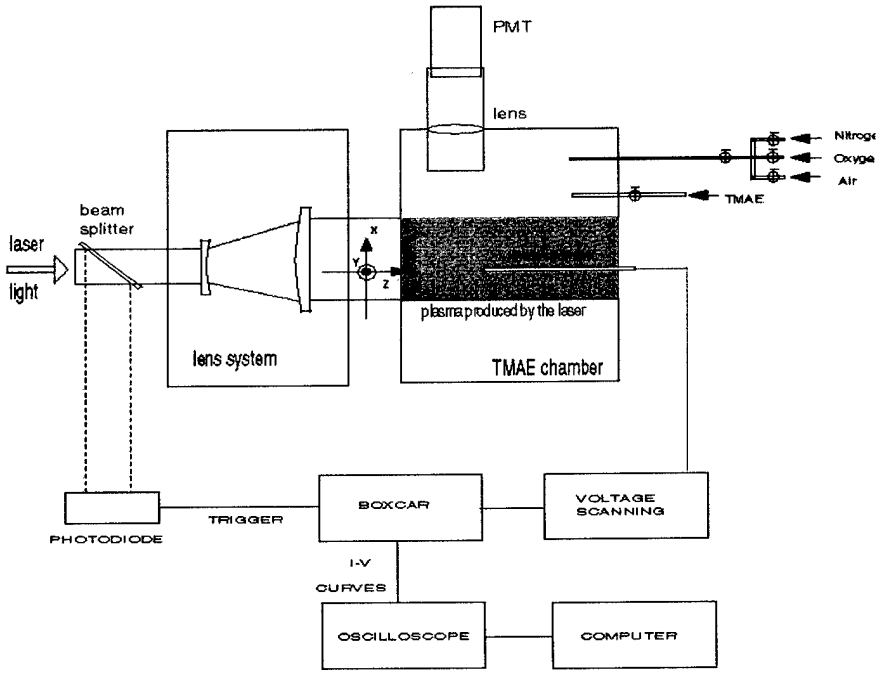

Fig. 2. Fast Langmuir probe characteristic measurement scheme.

B. Characterization of Laser Produced TMAE Plasma

(i) Fast Langmuir Probe Measurement

A large volume (hundreds of cm^3) plasma is created by a 193 nm laser ionizing an organic vapor, tetrakis (dimethyl-amino) ethylene (TMAE). The plasma is characterized as high electron density (10^{13} - $10^{12}/cm^3$) and low electron temperature (~0.1 eV) [1]. To investigate the plasma decay processes, a fast Langmuir probe technique is developed, including a detailed consideration of probe structure, probe surface cleaning, shielding, frequency response of the detection system, physical processes in probe measurement, dummy probe corrections as well as noise analysis. The mechanisms for the plasma decay are studied and a delayed ionization after the laser pulse is found to be important. This mechanism is also supported by optical emission measurements that nitrogen enhances the delayed emission from TMAE plasma. A model combining electron-ion recombination and delayed ionization is utilized together with experimental results to order the terms and calculate the relaxation times for delayed ionization. The relaxation times are longer for lower TMAE pressures and lower electron densities. For a source-free plasma, the density decay process is usually described as

$$\frac{dn_e}{dt} = -D\nabla^2 n_e - \alpha_{eff} n_e^2 - \nu_a \nu_e \qquad \text{(III.1)}$$

where D is plasma diffusion coefficient, α_{eff} is the effective recombination coefficient, and ν_a is the electron attachment frequency.

Electron-ion recombination

With the neglect of both diffusion and electron attachment processes, which are small in the experiment, Eq. (III.1) becomes

$$\frac{dn_e}{dt} = -\alpha_{eff} n_e^2 \qquad \text{(III.2)}$$

The solution to this equation is

$$\frac{1}{n_1} = \frac{1}{n_0} + \int_{t_0}^{t_1} \alpha_{eff}\, dt \qquad \text{(III.3)}$$

where n_0 and n_1 are the electron densities at times t_0 and t_1 respectively. The effective α_{eff} in this manuscript are approximately calculated from the corresponding electron densities at two successive measurement times.

$$\alpha_{eff} = \left(\frac{1}{n_1} - \frac{1}{n_0}\right) \Big/ (t_1 - t_0) \qquad \text{(III.4)}$$

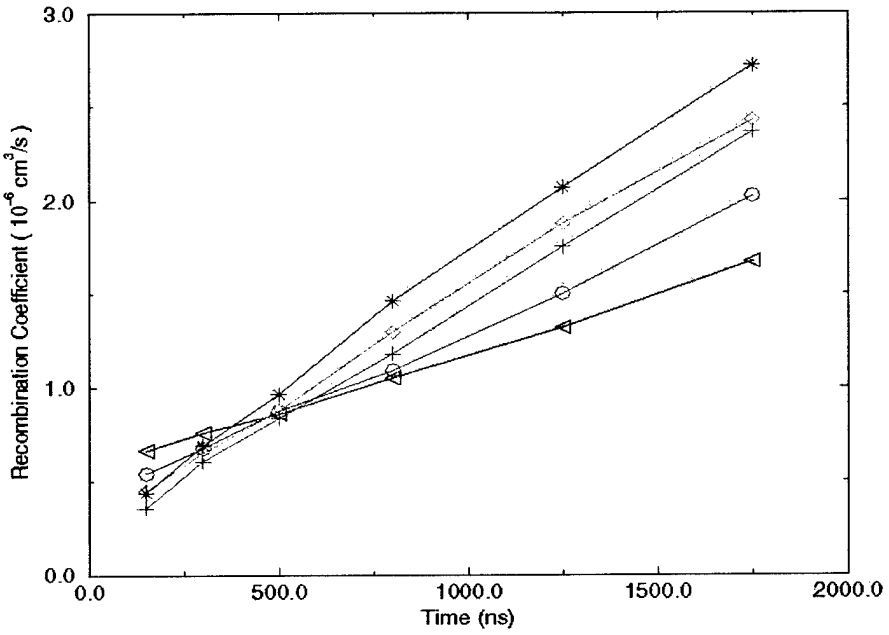

Fig. 3. Effective electron-ion recombination coefficient vs. time under conditions of 4mJ/cm^2 laser fluence with TMAE pressure of (*)16 mTorr, (◊)8 mTorr, (O)4 mTorr, (∇)2m Torr and under 8 mJ/cm^2 laser fluence with TMAE pressure of (+) 8 mTorr.

We plot α_{eff} versus time for different experimental conditions in Fig. 3. The results show that α_{eff} is not constant with time, but increasing. The higher the TMAE pressure, the more rapid is the increase in α_{eff} with time. Another result is that the change in α_{eff} is only weakly dependent on the change in electron temperature. One can write the first order relationship, due to electron temperature, as

$$\left|\Delta\alpha_{eff}\right| = \left|\frac{\partial\alpha_{eff}}{\partial T_e}\right| * \left|\Delta T_e\right| \qquad \text{(III.5)}$$

If the electron temperature T_e effect were important in the change in α_{eff} the larger $|\Delta T_e|$ should cause the larger $|\Delta\alpha_{eff}|$, but the experimental results in Fig. 4 shows the opposite. First, from t=100 ns to t= 2000 ns, $|\Delta T_e|$ for the 2 mTorr TMAE case is larger than that of 16 mTorr case, but $|\Delta\alpha_{eff}|$ in the 2 mTorr case is smaller than that of 16 mTorr case.

Second, for the 16 mTorr TMAE pressure case, T_e is almost constant in time (0.6 μs < t < 2 μs), but the α_{eff} is approximately tripled. These results show that the change in α_{eff} is only weakly dependent on the change in electron temperature. This agrees in general that for a larger molecular ion, α_{eff} is less electron temperature dependent, e.g. H_3O^+ (H_2O_2) and NH_4^+ $(NH_3)_2$ plasmas which are almost independent of T_e.

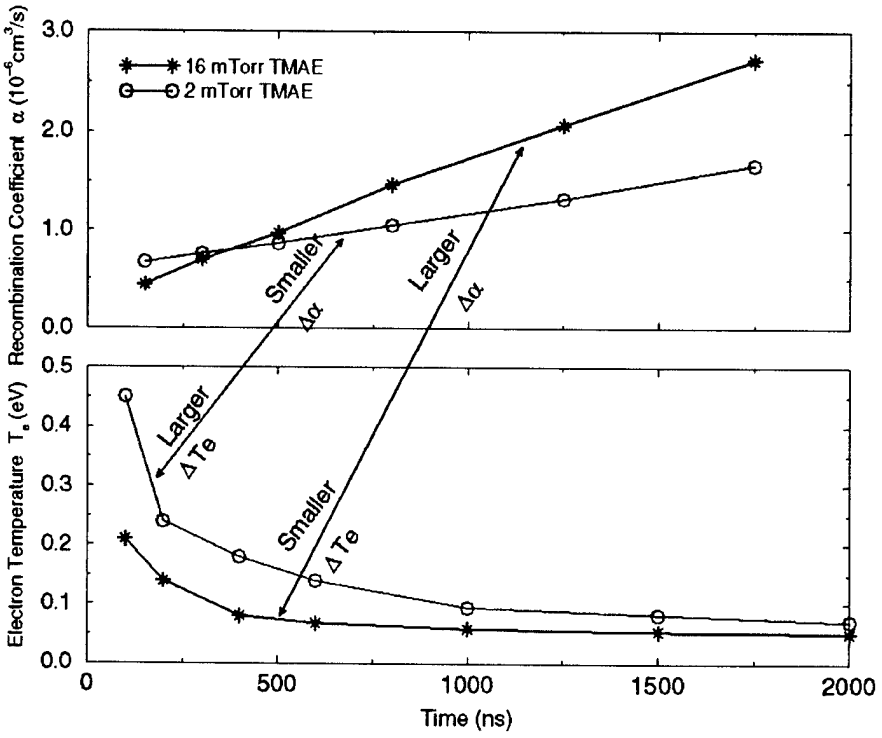

Fig. 4. Comparison of the variation of α_{eff} and T_e with time under conditions of 4 mJ/cm^2 laser fluence with TMAE pressures of 2 and 16 mTorr.

(a) Observation of Delayed Ionization in Laser Formed Plasma:

The delayed ionization mechanism can interpret the ``unexplained" experimental observations. (1) The delayed ionization decays rapidly with time, so it becomes less important during later times. This causes α_{eff} to increase with time. (2) As the TMAE pressure increases,

due to the collisional reaction TMAE+TMAE**, TMAE** decays more rapidly, so that the delayed ionization process is reduced. This is the reason that the plasma of 16 mTorr TMAE case decays more rapidly than that of 2 mTorr TMAE case. Second, the delayed optical emission experiments strongly support the delayed ionization interpretation, which will be presented in the next section. Third, there are many reports on delayed ionization phenomenon in laser ionization of large molecules. Fourth, TMAE super-excited phenomenon has been reported when excited from 185 nm to 196 nm, although the relaxation time of the delayed ionization is not measured. According to this report, when TMAE is excited by a 193 nm laser, superexcited TMAE** can be created. In sum, the mechanisms of the laser-produced TMAE plasma decay processes are studied, compared with the experimental measurements, and a delayed ionization process is indicated.

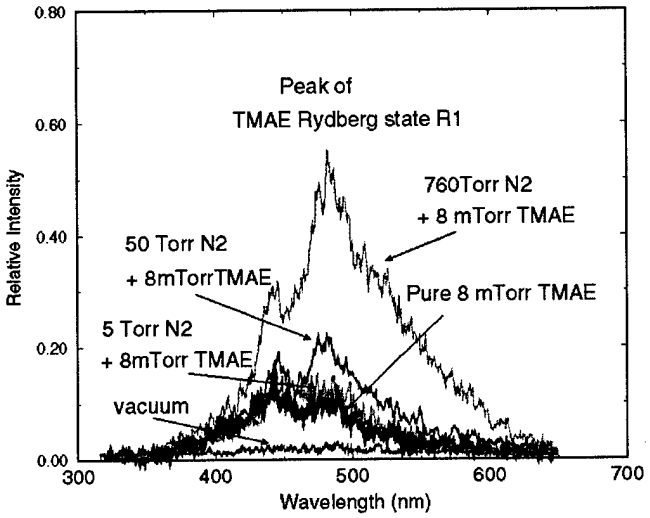

Fig. 5. Nitrogen effect on delayed emission from the laser produced TMAE plasma emission spectra, measured at time window of 300 ns <t< 130 ns after the laser pulse.

Two conclusions can be drawn from the relaxation time results from Fig. 5: (1) the relaxation time of the delayed ionization increases with time; (2) the relaxation time of the delayed ionization decreases with increasing TMAE pressure.

The relaxation time of the delayed ionization, τ, is quite comparable to the lifetime of the TMAE** state, because TMAE** is the source of the delayed ionization. The lifetime of

$TMAE^{**}$ can be influenced by the TMAE pressure and electron density due to collisions. Thus, the relaxation time τ is related to TMAE pressures and electron densities. As the electron density decreases with time, the rate of electron quenching of $TMAE^{**}$ decreases, so that the lifetime of $TMAE^{**}$ and the relaxation time of the delayed ionization increase with time. As TMAE pressure increases, the rate of TMAE molecular quenching of $TMAE^{**}$ increases, so that the relaxation time decreases.

In sum, with the assumption that electron density change is primarily due to electron-ion recombination and delayed ionization processes, a model is developed to calculate the relaxation time of the delayed ionization, which are longer under lower TMAE pressures and lower electron densities. This research has been published in the Physics of Plasmas [1].

(ii) A new application of 105 GHz mm Wave Interferometry

A 105 GHz (QBY-1A10UW, Quinstar Technology) quadrature-phase, millimeter wave interferometer is also used to characterize the temporal development of plasma following the application of the 20 ns laser pulse [2]. It accurately measures the plasma density and effective collision frequency at high neutral gas pressures [3]. The interferometer works in the Mach-Zehnder configuration, in which the plasma is in one arm of the two-beam interferometer. In low pressure discharges where the wave frequency (ω) is much greater than the plasma (ω_p) and the collision frequency (ν), a linear relationship exists between the plasma density and the phase shift. In this case the wave suffers almost little or no attenuation as it travels through the plasma. The phase difference between the two arms with the plasma present compared to that without the plasma is a measure of the plasma density [4]. However, at high gas pressures, where the collision frequency is comparable to both plasma and wave frequencies, the wave propagating through the plasma arm undergoes phase change as well as strong attenuation and both plasma density and effective collision frequency have a complex dependence on phase as well as amplitude changes. We have employed a measurement technique and a model where both phase and amplitude change data are used to uniquely determine the spatial average plasma density and effective collision frequency that is described in detail in Ref. [3]. The interferometer works by using an I-Q (In-phase and Quadrature phase) mixer to determine the phase and amplitude change of the 105 GHz mm wave signal going through the plasma. A fast

digital storage oscilloscope with advanced triggering capabilities (Lecroy 9354 series, 2 Gs/s) and GPIB interface is used to transfer detector diode signals to the computer. The entire interferometer assembly is enclosed in a conducting box with slots for waveguides. In order to minimize the noise level in the interferometer signal, semi-rigid co-axial cables with very efficient shielding (≥ 90 dB, Times Microwave Systems) have been used. We also checked that the effect of mm wave diffraction due to small plasma size was insignificant. The sequence of operation that includes charging the laser capacitor, firing the laser pulse and appropriate trigger of the fast oscilloscope for data acquisition is controlled by a program written in LabView. An axial density scan is obtained by varying the position of the interferometer along the z-axis. The interferometer trace shown in Fig. 2 is a function of time as the 35 mTorr TMAE plasma formed by the application of 20 ns laser pulse decays. Since the laser intensity is uniform ($\Delta I/I \sim 10\%$) over 2.8 cm diameter, a uniform radial plasma profile is assumed. A numerical program written in MATLAB solves simultaneously for both phase and attenuation data to obtain the average plasma density as well as the effective collision frequency.

(A) Plasma Decay Processes:

A sufficiently long plasma life-time after the application of the laser pulse is critical for an efficient transition to rf inductive wave coupling to sustain the plasma. The plasma life time will vary significantly for different background gases. The nature of the dominant loss mechanism can be obtained from the temporal plot of plasma density. Each point on the interferometer trace corresponds to the instantaneous line average plasma density and effective electron-neutral collision frequency. The instantaneous plasma density and corresponding effective collision frequency are obtained by simultaneously solving the instantaneous phase and amplitude change data. A plot of plasma density and effective collision frequency as a function of time is obtained. An estimate of the effective recombination rate for high-pressure discharges is also obtained by taking the time derivative of density. The continuity equation for pure TMAE plasma, including an ambipolar diffusion term, an ionization frequency term, ν_{iz}, and two-body and three-body recombination terms is given by the following equation [5],

$$\frac{\partial n_e}{\partial t} = D_n \nabla^2 n_e + \nu_{iz} n_e - \alpha_r n_e^2 - \beta_r n_e^2 . \qquad \text{(III.6)}$$

Here, α_r is the two-body (electron-ion) recombination coefficient and β_r ($\sim\beta_g+\beta_e$) is the three-body recombination coefficient involving either a neutral atom (β_g) or an electron (β_e) as the third particle. Since the TMAE molecule is a strong electron donor, the electron attachment in pure TMAE plasma is very small and is neglected. As we are interested in the plasma decay properties after the application of the laser pulse, the density decay in the absence of any ionizing source is given by,

$$\frac{\partial n_e}{\partial t} = D_n \nabla^2 n_e - \alpha_r n_e^2 - \beta_r n_e^2 . \qquad \text{(III.7)}$$

The diffusive loss in a pure TMAE plasma after the application of the 20 ns laser pulse is small on the μs time scale as measured by Ding et. al. [1]. Therefore, for a temporally decaying TMAE plasma, the continuity equation takes the form

$$\frac{\partial n_e}{\partial t} \approx -\alpha_r n_e^2 - \beta_r n_e^2 . \qquad \text{(III.8)}$$

The effect of three-body recombination is small in the pressure range 4-50 mTorr. The three-body recombination process where the third body is an electron, i.e., $A^+ + e + e \rightarrow A^* + e$, electrons are captured by ions to form excited neutrals. These excited atoms relax to the ground states through electron impacts and radiative emission. The recombination coefficient for this process is $\kappa_e \approx 1.64\times10^{-9}\{T(K)\}^{-9/2}$ cm^6/s [6]. For electron densities $n_e \sim 10^{13}$cm^{-3} at room temperature, the recombination coefficient is $\beta_e=\kappa_e n_e \sim 10^{-7}$ cm^3/s. The neutral-stabilized electron-ion collisional recombination process, $A^+ + e + B \rightarrow A^* + B$, where B is a neutral atom, is important only at high neutral gas densities. The classical reaction rate constant for this process is given by [7]

$$\kappa_r \sim 6\times10^{-27}\left(\frac{300}{T(K)}\right)^{1.5} (\text{cm}^6/\text{s}) \qquad \text{(III.9)}$$

Here T is the temperature in degree Kelvin. For pure TMAE plasma at maximum pressure of 50 mTorr at 300 K ($n_g \approx 1.6\times10^{15}$ cm^{-3}), the recombination coefficient is $\beta_g=\kappa_r n_g \sim 9.6\times10^{-12}$ cm^3/s and can be neglected. In general, the temperature dependence of the recombination coefficient varies for different gases. In this work the rate coefficient for nitrogen, carbon dioxide and water vapor is taken from Bates [8]. It is given as $\kappa_r(N_2)\sim1.6\times10^{-}$

$^{26}(300/T)^{2.5}$ cm^6/s, ,$\kappa_r(CO_2)$~$5.7\times10^{-25}(300/T)^{1.3}$ cm^6/s, and ,$\kappa_r(H_2O)$~$8\times10^{-23}(300/T)^{4.2}$ cm^6/s. Therefore, in the presence of molecular background gas at atmospheric pressures this contribution is significant and is included.

Therefore, three-body recombination $A^+ + e + e \rightarrow A^* + e$, for pure TMAE plasma, can be incorporated by defining an effective recombination coefficient (α_{eff}) that can be readily determined from the temporal plot of plasma density. The continuity equation then becomes

$$\frac{\partial n_e}{\partial t} = -(\alpha_r + \beta_e) n_e^2 = -\alpha_{eff} n_e^2 . \qquad \text{(III.10)}$$

The functional form of the solution is

$$n_e(t) = \frac{n_e(0)}{1 + \alpha_{eff} n_e(0) t} \xrightarrow[t\to\infty]{} \frac{1}{\alpha_{eff} t} \qquad \text{(III.11)}$$

where $n_e(0)$ is the initial TMAE plasma density at time t=0.

Ding et. al.[1] have also reported that in addition to the process of direct ionization $AB + h\nu \rightarrow AB^+ + e$, the phenomenon of delayed ionization plays an important role in the TMAE plasma formation and subsequent decay process. Since the quantum efficiency of TMAE is 30%, [9] some of the photons absorbed by TMAE molecules do not contribute to the direct ionization and instead these photons produce excited neutrals. By electron impact, these excited neutrals ionize (delayed ionization) or dissociate through the processes

$$AB + h\nu \rightarrow AB^* \rightarrow \begin{cases} AB^+ + e \ (\textit{delayed ionization}) \\ A + B \qquad (\textit{dissociation}) \end{cases} \qquad \text{(III.12)}$$

The process of delayed ionization can be incorporated in the temporal TMAE plasma density decay as,

$$\frac{\partial n_e}{\partial t} = -\alpha_{eff} n_e^2 + D . \qquad \text{(III.13)}$$

Here D, the delayed ionization coefficient, is assumed a constant. The solution in terms of hyperbolic tangents is

$$n_e(t) = \sqrt{D/\alpha_{eff}} \tanh\left\{ t\sqrt{\alpha_{eff}}\sqrt{D} + \tanh^{-1}\left(n_e(0)\sqrt{\alpha_{eff}/D} \right) \right\} \qquad \text{(III.14)}$$

The experiment is performed to investigate the TMAE plasma decay characteristics in the presence of the background gas. The presence of oxygen, as a constituent of the background gas and as an impurity, results in plasma losses due to three-body electron attachment with oxygen. The modified continuity equation is

$$\partial n_e/\partial t = -\alpha_r n_e^2 - \beta_r n_e^2 - \kappa_a n_e n_g^2. \qquad \text{(III.15)}$$

Here κ_a is the three-body electron attachment rate constant for the process $e + TMAE^+ + O_2 \rightarrow O_2^- + TMAE$. These negative ions are subsequently removed by ionic recombination causing fast quenching of TMAE plasma. n_g is the neutral particle density of the background gas. TMAE partial pressure being small, it is reasonable to assume that we have only background gas neutral particles. Since the background gas is at atmospheric pressure, neutral particle density is high and as a result the contribution of three-body recombination involving neutrals as the third particle becomes important. Using the definition of an effective recombination coefficient,

$$\partial n_e/\partial t = -(\alpha + \beta_r)\, n_e^2 - \kappa_a n_e n_g^2$$

$$= -\alpha_{eff} n_e^2 - \nu_a n_e \qquad \text{(III.16)}$$

Here ν_a is the electron attachment frequency. The plasma density decays accordingly as,

$$n_e(t) = -\frac{\nu_a n_e(0)}{\alpha_{eff} n_e(0)\left(1 - \exp(\nu_a t)\right) - \nu_a \exp(\nu_a t)}. \qquad \text{(III.17)}$$

These loss parameters are determined from the temporal plots of plasma density.

(iii) Density Decay and Recombination Rates

A large volume (~500 cc), high density TMAE plasma is created by single photon 193 nm laser photo-ionization in a plasma chamber. The plasma chamber is evacuated to a base pressure of 10^{-6} Torr using a turbo-molecular pump. The TMAE pressure is raised to the desired value (4-50 mTorr) in this evacuated chamber by opening a TMAE liquid filled bottle at room temperature, while continuing to pump at a slow rate. In order to increase the TMAE vapor pressure, hot air is blown on to the TMAE bottle. Plasma density and effective collision frequency are determined from both phase and amplitude change data. These quantities are

further used to determine the effective recombination coefficient as well as the density decay rate.

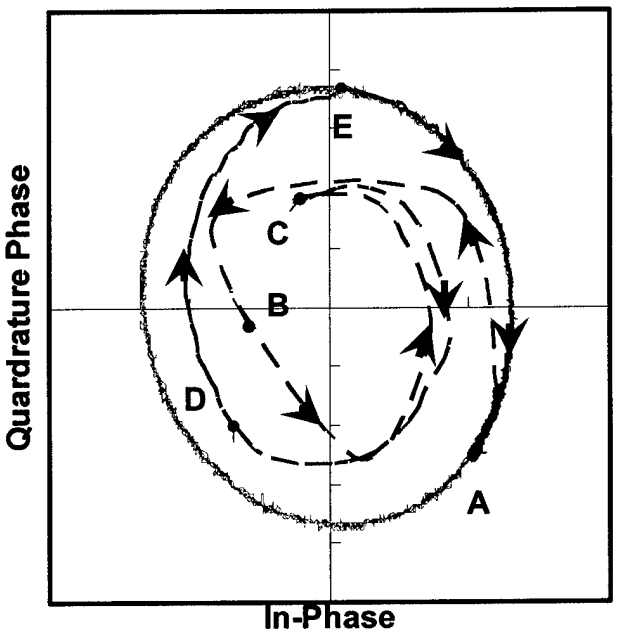

Fig. 6. Interferometer trace showing the phase and amplitude variation for 35 mTorr TMAE plasma during 20ns laser pulse reaching a maximum line-average plasma density of 4×10^{13} cm^{-3} (A→B→C), followed by the plasma decay (C→D→E→A) at a distance of 20 cm from the laser window. The outside circle represents the vacuum phase variation.

The interferometer trace showing the phase and amplitude variation for a 35 mTorr TMAE plasma is presented in Fig. 6 and the temporal plot of the plasma density corresponding to the interferometer trace is shown in Fig. 7. The outside circle in Fig. 6 represents the phase variation for the vacuum condition. The onset of plasma follows the path A→B→C. The plasma is formed by the application of the 20 ns laser pulse and during this interval the line average plasma density reaches its maximum value of 4×10^{13} cm^{-3}. After the application of the laser pulse, the TMAE plasma decays temporally along the path C→D→E→A.

In Figure 8, the temporal plot of TMAE plasma density for different TMAE vapor pressures is shown. It is observed that the plasma density increases with the vapor pressure, however, the plasma density decay is more rapid at higher vapor pressure. Note that during the early times for about 100 ns after the formation of plasma, the density decay depends on the initial density and the two-body process involving electron-ion recombination plays the

dominant role. Following the initial decay, the plasma density approaches an equilibrium value for all three vapor pressures. For time > 100 ns, the density decay curves are similar for both 6 mTorr and 10 mTorr case. In contrast the density decay curve for 50 mTorr shows more rapid decay for this time interval. This is also evident in the temporal plot of recombination coefficient shown in Fig. 12.

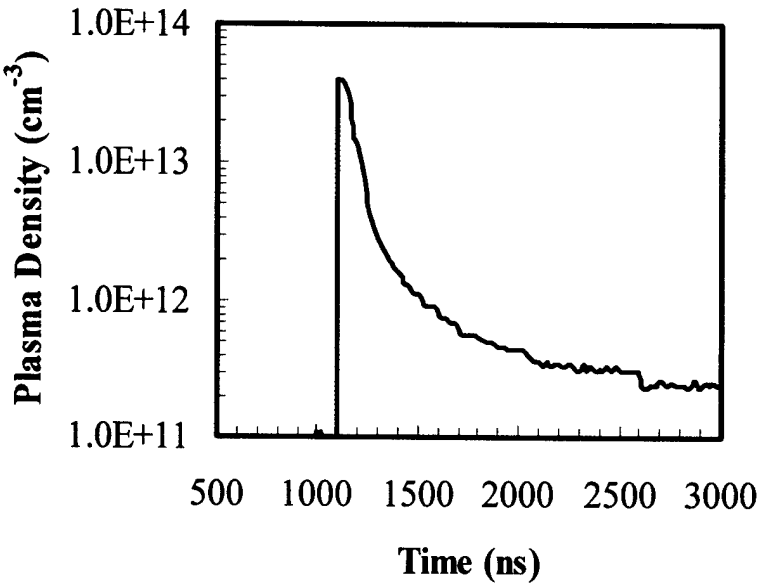

Fig. 7. Temporal plot of the line-average plasma density at 35 mTorr TMAE corresponding to interferometer trace shown Fig. 2.

The plasma density for different TMAE vapor pressures at different axial positions from the laser window is shown in Fig. 9 and the corresponding axial density decay plot is shown in Fig. 10. The laser flux for these measurements is held constant at 6 mJ/cm^2. The size of the vertical bar shown in fig. 9, for axial distance Z=20 cm from the laser window, represents the percent variation over 10 shots. Plasma density at TMAE vapor pressures less than 4 mTorr could not be seen on the interferometer trace. It is also shown in the plot that after an initial increase in the peak TMAE plasma density with increasing vapor pressure, the increase in peak plasma density with pressure is small above 40 mTorr. At 20 cm from the window, there is a two-fold increase in line-average peak density from 1.4×10^{13} cm^{-3} at 4 mTorr to 2.8×10^{13} cm^{-3} at 10 mTorr, and from 4.5×10^{13} cm^{-3} at 40 mTorr it increases slightly to 4.7×10^{13} cm^{-3} at 50 mTorr.

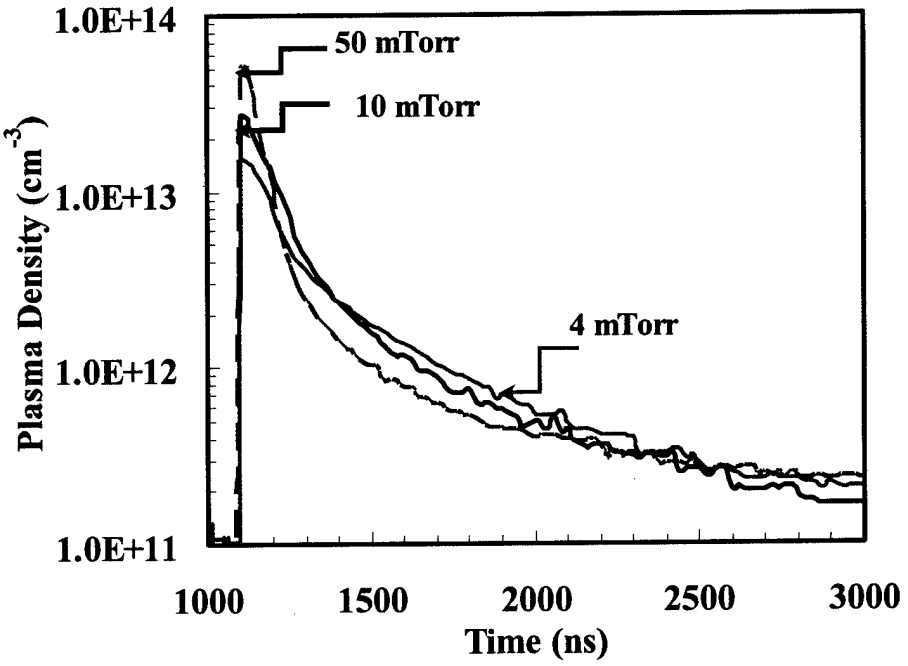

Fig. 8. TMAE plasma density versus time plot for at different TMAE vapor pressures.

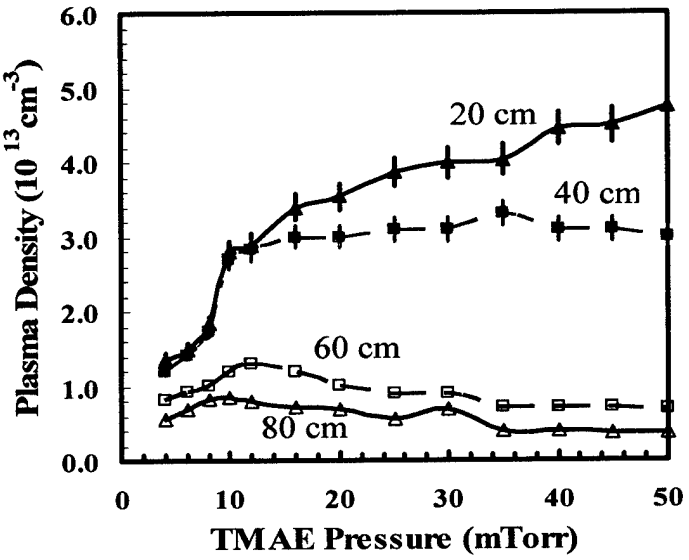

Fig. 9. TMAE plasma density versus TMAE vapor pressure at axial distances measured from the laser window for a fluence of 6 mJ/cm^2.

The axial plasma density plot in Fig. 10 reveals a sharp plasma density decay for higher vapor pressure plasmas. The fractional plasma density at an axial location of 80 cm with respect to its value at 20 cm is 40%, 30%, 14% and 8% for the 4, 10, 30 and 50 mTorr cases, respectively. This is due to the enhanced laser absorption near the Suprasil window at higher pressures.

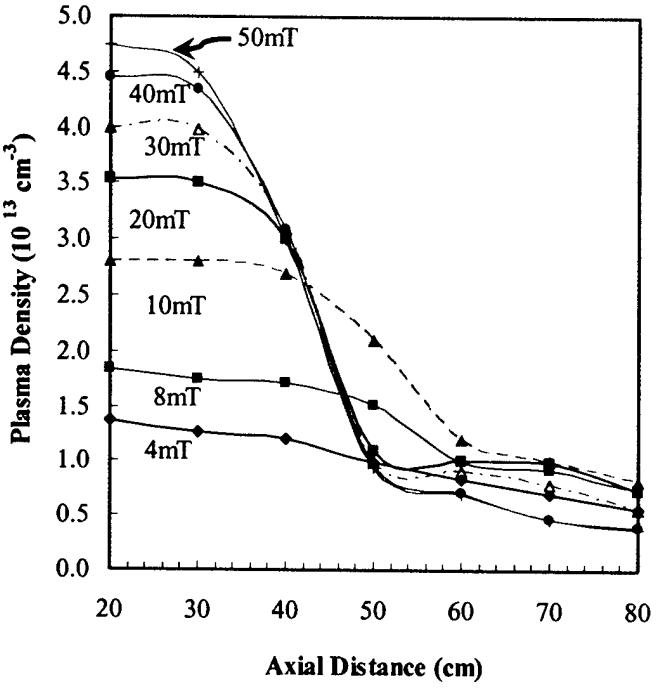

Fig.10. Axial density plot for various TMAE vapor pressures for a laser fluence of 6 mJ/cm^2.

In order to study the effect of background gases on the TMAE plasma formation and decay characteristics, the plasma chamber was raised to the atmospheric pressure by introducing a particular gas. The TMAE bottle was pressurized with argon gas and an electromechanically actuated valve was used to introduce doses of pressurized TMAE to the background gas. The doses were adjusted such that a TMAE vapor pressure of 16 mTorr is obtained. The TMAE vapor pressure for a given dose is verified by introducing the pressurized TMAE vapor into an evacuated chamber and by measuring the peak plasma density. A temporal plot of TMAE plasma density in the presence of different background gas is shown in Fig. 11. A laser fluence of $4mJ/cm^2$ is maintained. Temporal variation of 16 mTorr TMAE plasma density is also shown in the plot for reference. The TMAE peak plasma density is 3.2×10^{13} cm^{-3}. In the presence of noble gases such as helium and argon, the TMAE peak

plasma density reduces to 2.9×10^{13} cm^{-3} and 2.3×10^{13} cm^{-3} respectively. It corresponds to a fractional drop of ~10% for helium and ~30% for argon background gas. It is also observed that a high density ($\sim10^{12}cm^{-3}$) plasma is maintained in the presence of noble background gas for over 2 μs. Since the background gas is at atmospheric pressure with neutral particle density ~ 2.5×10^{19} cm^{-3}, the effect of three-body recombination involving a neutral as the third particle becomes an important factor. In the experiment with air constituents as the background gas, the effect of electron attachment is evident. The peak TMAE plasma density obtained in the presence of nitrogen, oxygen and air is 1.8×10^{13} cm^{-3}, 5.8×10^{12} cm^{-3} and 9.85×10^{12} cm^{-3} respectively. Higher TMAE density can be obtained by increasing the TMAE vapor pressure and the laser fluence. The TMAE plasma life-time in excess of 100 ns with air is long enough so that rf power can be coupled efficiently.

A. Plasma Decay

No single loss mechanism can possibly explain the TMAE plasma decay in all the three experimental conditions viz., pure TMAE and TMAE seeded in noble gas and air constituent gas. After the application of the 20 ns pulse, TMAE plasma decays mainly through two-body electron-ion recombination, three-body recombination with a neutral as the third particle and the electron attachment process. In the following section, we describe the dominant loss process and present the calculation of recombination parameters using the TMAE plasma density decay plots shown in Figs. 8 and 11.

(a) Pure TMAE Plasma

The effective recombination coefficient for pure TMAE plasma can be measured from the temporal plot of plasma density. A numerical solution of Eq. (III.5) is obtained by determining the electron densities n_0 and n_1 at two successive time measurements t_0 and t_1 respectively. It is given as,

$$\frac{dn/dt}{n^2} \approx \frac{n_0 - n_1}{n_0 n_1 (t_1 - t_0)} = \alpha_{eff} \qquad \text{(III.13)}$$

Since TMAE is a strong electron donor, contribution of electron attachment to the plasma decay process is ruled out. In addition with TMAE partial pressure ~ 4-50 mTorr, three-body recombination contribution is also negligible. Therefore, one can reasonably

conclude that $\frac{dn/dt}{n^2}$ term in Eq. (III.13) refers to two-body electron-ion recombination coefficient α_{eff}. Using the data from the temporal density plot in Fig.4, a temporal plot of α_{eff} is shown in Fig. 13.

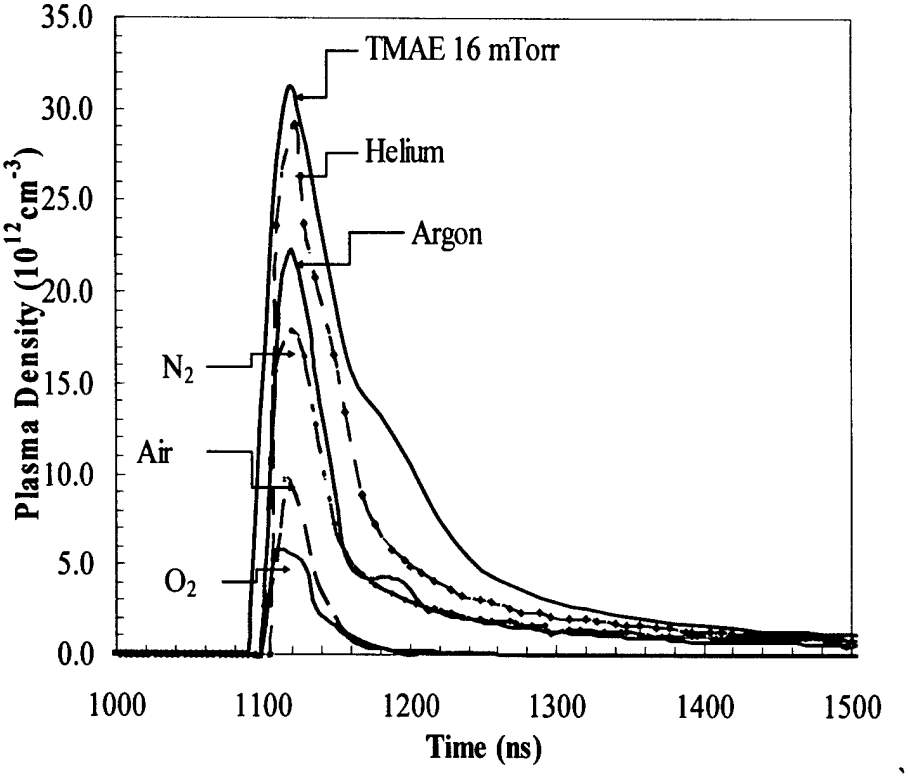

Fig. 11. TMAE plasma density versus time plot for different background gases at 760 Torr

As shown in the plot, the recombination coefficient increases with time. It also shows more rapid initial increase in α_{eff} for higher TMAE vapor pressure. This result is in agreement with the earlier study carried out by Ding. et. al.,[1]. This increase in α_{eff} with time can be explained in terms of the process of delayed ionization described in Eq. (III.7) and (III.8).

(b) Background Noble Gas

In the presence of a noble gas at 760 Torr, three-body recombination involving neutrals as the third particle becomes important. Neglecting electron attachment, Eq.(III.10) can be expressed as,

$$\frac{dn/dt}{n^2} \approx \frac{n_0 - n_1}{n_0 n_1 (t_1 - t_0)} = \alpha_{eff} + \beta_r \qquad \text{(III.14)}$$

Here α_{eff} represents the effective recombination coefficient for TMAE alone. In Fig. 13, a temporal plot of $\frac{dn/dt}{n^2}$ is shown for TMAE plasma in the presence of background gases. Using the data presented in Fig.13, three-body recombination coefficient in the presence of argon and helium is obtained. A plot of $\kappa_r(=\beta_r/n_g)$ is presented in Fig.14. Since the three-body recombination process depends on the neutral gas density, maintained constant during the experiment, we observe a very small temporal variation of κ_r. The small variation is within the statistical error. In this experiment, the three-body recombination rate coefficient for TMAE in the presence of helium and argon is determined to be (3.6-5.1)×10^{-26} cm^6s^{-1} and (8.8-10.2)×10^{-26} cm^6s^{-1} respectively.

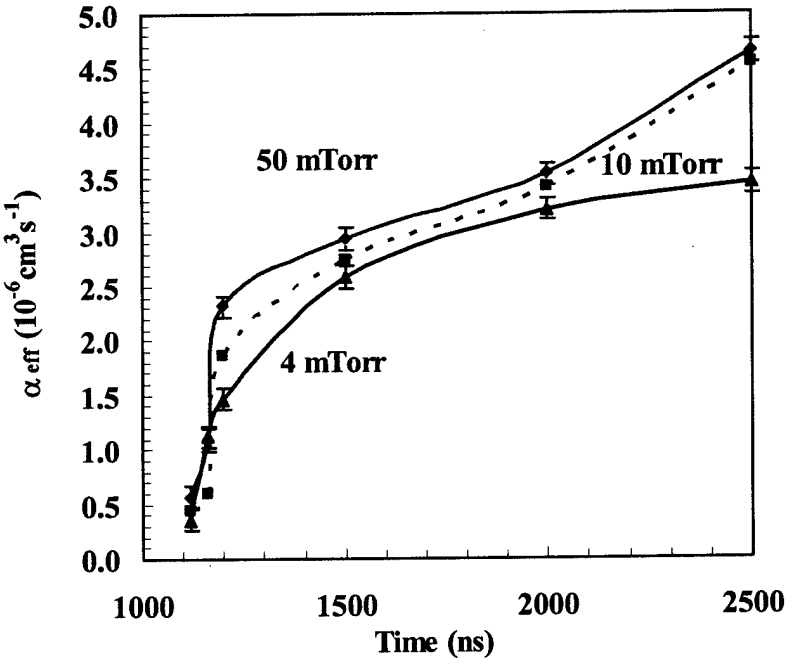

Fig. 12. Temporal plot of recombination coefficient for TMAE plasma

(c) Background Air Constituent Gases

In atmospheric pressure air, the dominant plasma loss mechanism is the electron attachment with oxygen through the process, $e + TMAE^+ + O_2 \rightarrow O_2^- + TMAE$. Negative

oxygen ions are removed by ionic recombination and this results in significant reduction of plasma life-time. In order to determine the electron attachment rate coefficient numerically, we use the density decay equation in Eq. (III.10). It is written as,

$$\frac{dn/dt}{n^2} \approx \frac{n_0 - n_1}{n_0 n_1 (t_1 - t_0)} = \alpha_{eff} + \beta_r + \frac{\kappa_a n_g^2}{n} \qquad \text{(III.15)}$$

Here κ_r ($=\beta_r/n_g$) is the three-recombination rate coefficient with oxygen and nitrogen as the third particle and κ_a is the electron attachment rate coefficient. Electron attachment rate coefficient based on the classical diffusion model includes the elastic scattering of electrons by the diatomic molecules by incorporating the excitation of vibrational and rotational levels. The κ_r value for nitrogen is given by Bates as $\sim 1.6\times10^{-26}\left(300/T\right)^{2.5}$ cm^6s^{-1} [8], where T is temperature in Kelvin. For hydrogen molecule we have taken κ_r value from Biberman et. al. [10] and it is $\sim 2\times10^{-26}$ cm^6s^{-1} at room temperature. The small difference in κ_r values is due to the mirror symmetry in molecules like oxygen, nitrogen and hydrogen that have no permanent dipole moments. In addition, the plasma decay through electron attachment with oxygen will be the dominant loss process in the presence of oxygen and air background gas. Therefore, in the present calculation we have reasonably assumed κ_r to be $\sim 10^{-26}$ cm^6s^{-1} for air as well as oxygen.

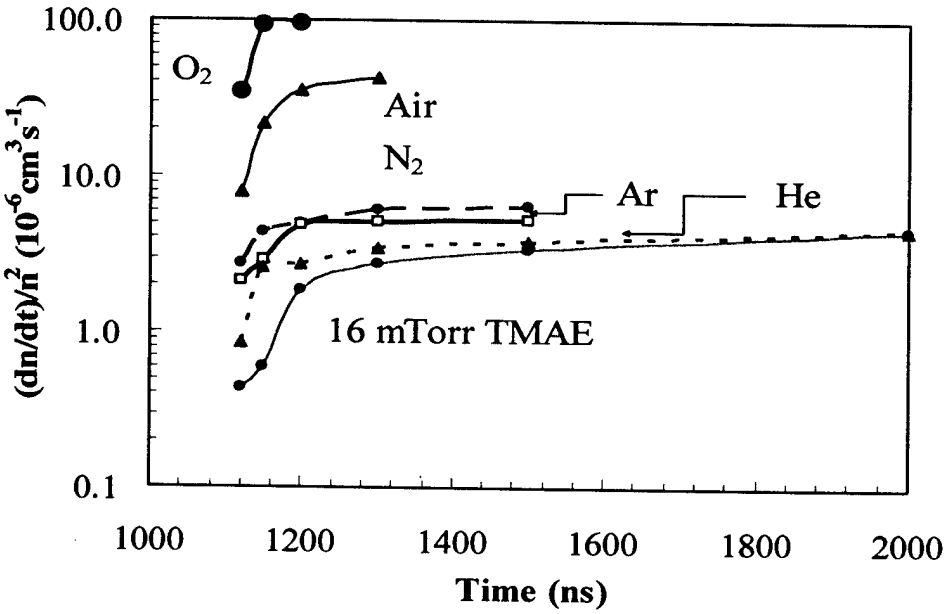

Fig. 13. TMAE plasma density decay coefficient for different background gases at 760 Torr.

The term $\frac{dn/dt}{n^2}$ for TMAE plasma in the presence of nitrogen, oxygen and air along with α_{eff} for 16mTorr TMAE plasma obtained from Fig. 13, is used to determine the electron attachment rate coefficient. A time plot of κ_a for nitrogen, oxygen and air is shown in Fig. 15.

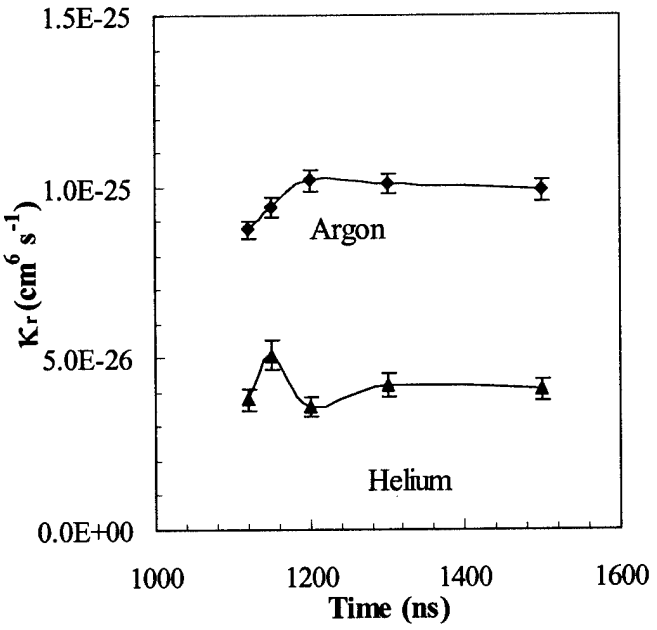

Fig. 14. Three-body recombination rate coefficient for TMAE plasma in the presence of helium and argon at 760 Torr.

One can see that the electron attachment rate decreases temporally with TMAE plasma density showing thereby, that the probability of electron capture for attachment decreases with the decrease in plasma density. Since the electron attachment rate for nitrogen immediately after the application of laser pulse is only 5.8×10^{-32} cm^6s^{-1}, the subsequent contribution to the plasma loss through electron attachment process is also very small. This is expected as nitrogen does not readily form a negative ion and this plasma loss can be attributed to the presence of oxygen impurity. However, for oxygen the electron attachment rate coefficient 3.3×10^{-31} cm^6s^{-1} is almost an order of magnitude higher. The plasma electron life-time in oxygen is $\tau_a=1/\nu_a=$ 5.1×10^{-9} s. κ_a with atmospheric air is 1.18×10^{-31} cm^6s^{-1} and the TMAE plasma life-time with respect to electron attachment in air is 1.4×10^{-8} s. This result is in agreement with the value of 1.1×10^{-8} s for air mentioned in the literature [6].

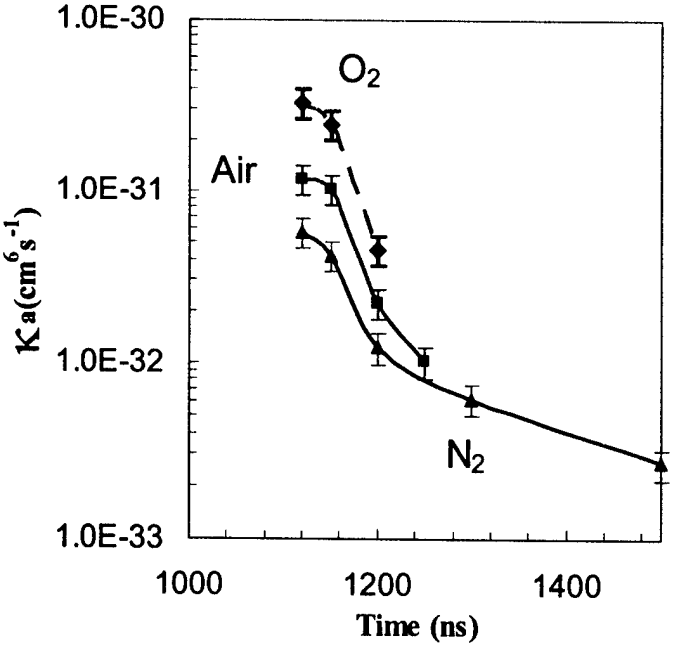

Fig.15. Electron attachment rate coefficient for TMAE plasma in the presence of nitrogen, oxygen and air at 760 Torr.

IV. Laser Initiated, Radio-Frequency Sustained Discharges

At higher pressures, there is a decrease in the mean electron temperature at constant radio-frequency (rf) power and fewer high-energy electrons are present. This effect, in addition to the increasing collision frequency due to high gas pressures, makes the energy cost per electron-ion pair created prohibitively high. The radio-frequency power required to initiate a discharge at high gas pressure (>100 Torr) is very high. However, once the gas breakdown has occurred and discharge is initiated, the rf power can be much more efficiently absorbed by the plasma through inductive coupling of the wave. We have also initiated the discharge at lower pressure and slowly increase the gas pressure and rf power but the time scale for creating high-pressure plasma from the low pressure discharge is several minutes.

Therefore, there is a need of an alternative scheme to bring down the power budget required to initiate and sustain the discharge at higher gas pressures. We hypothesized that if

we could ionize a seed gas (~8 mTorr of tetrakis (dimethylamino) ethylene or TMAE) by (193 nm) ultraviolet laser photon absorption, then we could efficiently couple radio frequency power to the plasma at higher gas pressure and sustain the plasma with modest radio frequency power. The laser preionized plasma provides an initial plasma impedance to the rf and improves the coupling significantly.

TMAE is an excellent choice as seed for laser preionization. TMAE has large photo ionization cross-section and higher rate constant for ionizing collision (Fig.16). In addition, its vertical ionization potential of 6.1 eV is well below that of the background gas. We have found that the liquid form of TMAE is compatible with air over long times and the vapor form can be used in air for several minutes. In some cases the emission from the gas phase TMAE and oxygen is very long lived and is measurable even after 30 minutes [11]. The organic gas TMAE can be considered as a seed in air by pulsed injection and fast laser or UV flash tube ionization for plasma initiation.

The most effective antenna for initiating and maintaining the plasma in this study is the five-turn helical coil, which excites the m=0 TE mode of field distribution The inductive coil consists of 5 turns of quarter-inch copper tubing wound tightly around the plasma chamber, giving an inner radius of 3.0 cm. The total length of the antenna is 13 cm. The measured value of the vacuum reactance of this antenna is much higher than the previous two antennas at 72 Ω at 13.56 MHz.

The maximum power absorbed occurs when $\beta R \approx 2.5$. It is evident that the value of βR in this experimental case is reduced by approximately an order of magnitude. There is a minimum βR at which the discharge can be maintained. For every value of current, $\lim_{\beta R \to 0} P_{abs}=0$. Meanwhile, P_{loss} never goes to zero because there are always ohmic losses in the antenna. The discharge can not be maintained when the ohmic losses in the antenna are greater than the radiation resistance of the antenna ($R_{loss} > R_r$). The vacuum impedance of the antenna was measured with the network analyzer to be $Z_{ant} = 0.02 + i72\ \Omega$. According to ANTENA calculations, the maximum pressure at which this antenna can maintain the discharge is about 500 Torr since the radiation resistance is 0.02 Ω for this pressure at a density of $n_e = 4\times10^{12}\ cm^{-3}$.

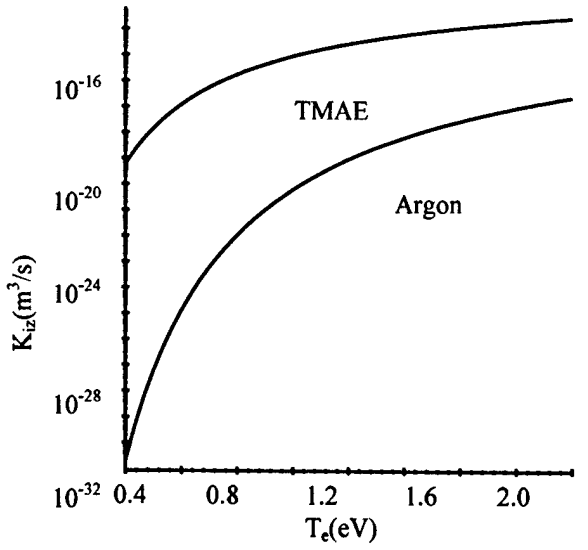

(a)

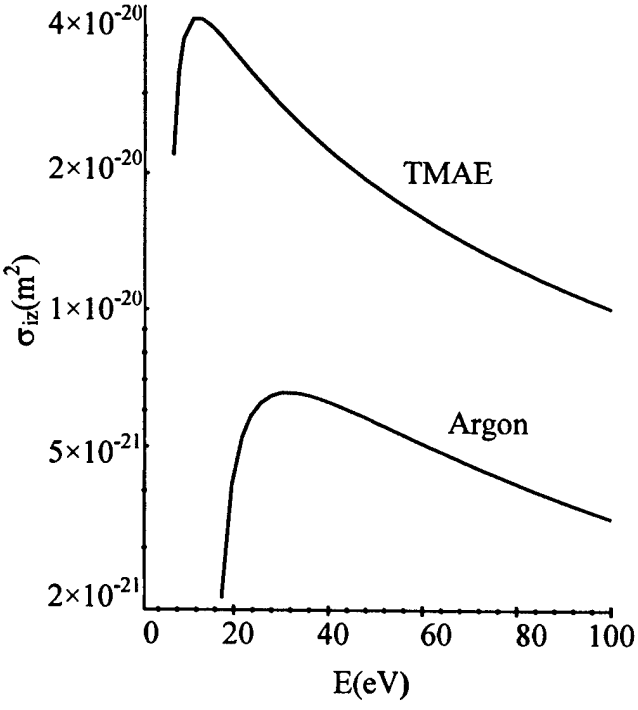

(b)

Fig. 16. (a) Rate Constants K_{iz} for ionizing collision and (b) classical Thompson ionization cross-section for TMAE and argon.

An experiment similar to the one carried out with the type-III antenna shows that the helical coil can capacitively ignite the discharge at pressures of up to 80 Torr with 2.8 kW of power. One interesting aspect that this antenna has over the other antennas studied is that the

electric field lines, which the electrons nearly follow, have only an azimuthal component, and close on themselves. This eliminates the radial component of the current density thought to be a major loss mechanism in the previous antennas which excited the m=1 modes.

Earlier experiments in our group have shown that a plasma with electron density ~ $4x10^{13}$ cm^{-3} can be produced in 2-8 mTorr of TMAE. We have also observed that the plasma lifetime of laser ionized TMAE is extended due to delayed ionization of super excited states by addition of up to 760 Torr of nitrogen [1]. In our earlier study we confirmed the viability of this scheme by initiating a discharge by laser preionization of 2-5 mTorr of TMAE seeded in 150 Torr of argon and sustaining the plasma at an RF power of 2.8 kW [5] whereas we could create plasma only up to 80 Torr with RF power alone. The plasma density scan with pressure at different sustaining RF power is shown in Fig. (17).

Recently we have made significant improvement in the experimental systems by redesigning the capacitive matching network, reducing the ohmic losses in the joints and improvising the gas injection system. In addition a very accurate, computer controlled timing circuit to sequence the steps of seed gas injection, laser firing, the RF enable and data acquisition has been designed and operated. This exact timing sequence is very critical since the RF pulse must be enabled during the TMAE plasma life time, so that the RF sustainment can take place. RF coupling depends critically on the presence of TMAE plasma and it will be significantly affected if the RF pulse is turned on before the laser preionization of TMAE or if it is turned on sufficiently late after the short TMAE plasma life time. In the evacuated plasma chamber, a small amount of TMAE is introduced with the pump gate valve closed and then pressure is raised to the desired value by introducing a background gas like argon. The flow condition here is similar to the static case and is used as a reference to measure the comparable efficiency of the scheme.

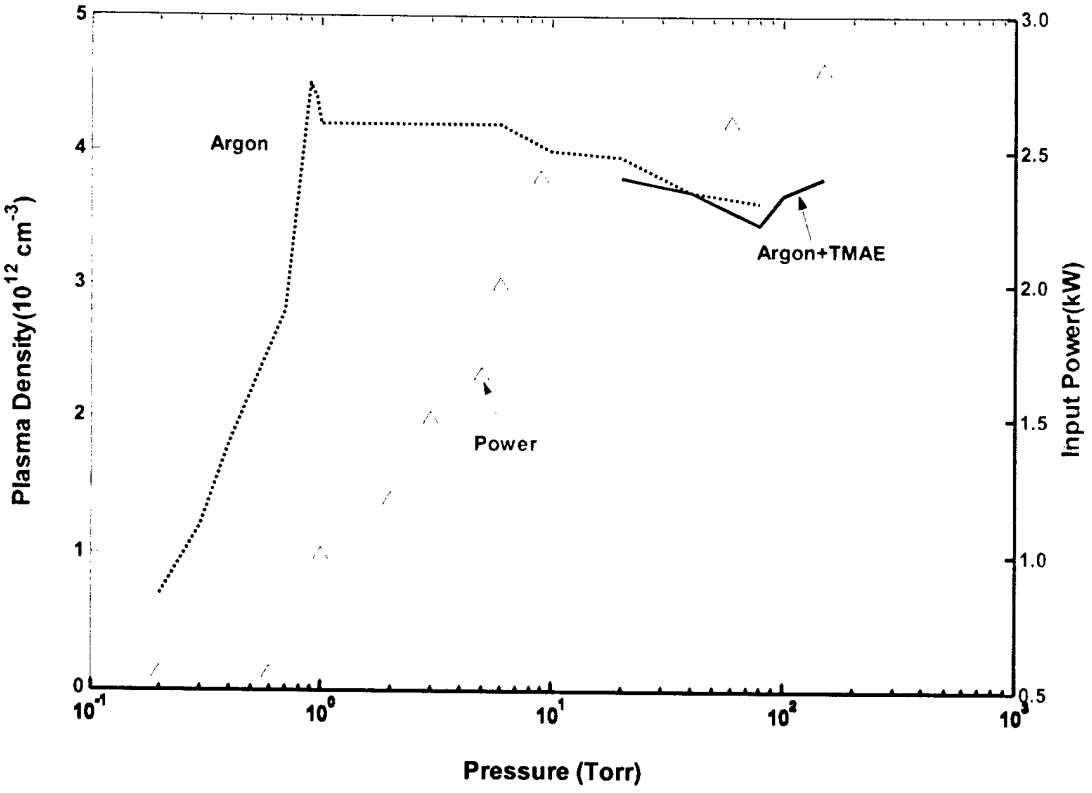

Fig. 17. Corrected plasma density vs. pressure for the five-turn helical antenna in argon and a TMAE/argon mixture.

With new improvements in the experimental systems and rf power (~ 2 kW); we were able to create a plasma up to 250 Torr in a 10 cm diameter chamber with RF power alone. Whereas we were able to initiate a laser preionized discharge of 5-10 mTorr of TMAE seeded in argon at 100-760 Torr and then sustained at modest RF power of 2 kW. A large volume plasma (~2500 cm^3) with high densities (n_e~10^{13}-$10^{12}$$cm^{-3}$) is obtained in a plasma chamber of 10 cm diameter. Plasma density measured 10 cm from the antenna at different gas pressure for a given power for two different cases has been plotted in Fig.19. We have recently improved the experimental system to obtain an axial scan of the interferometric density measurements.

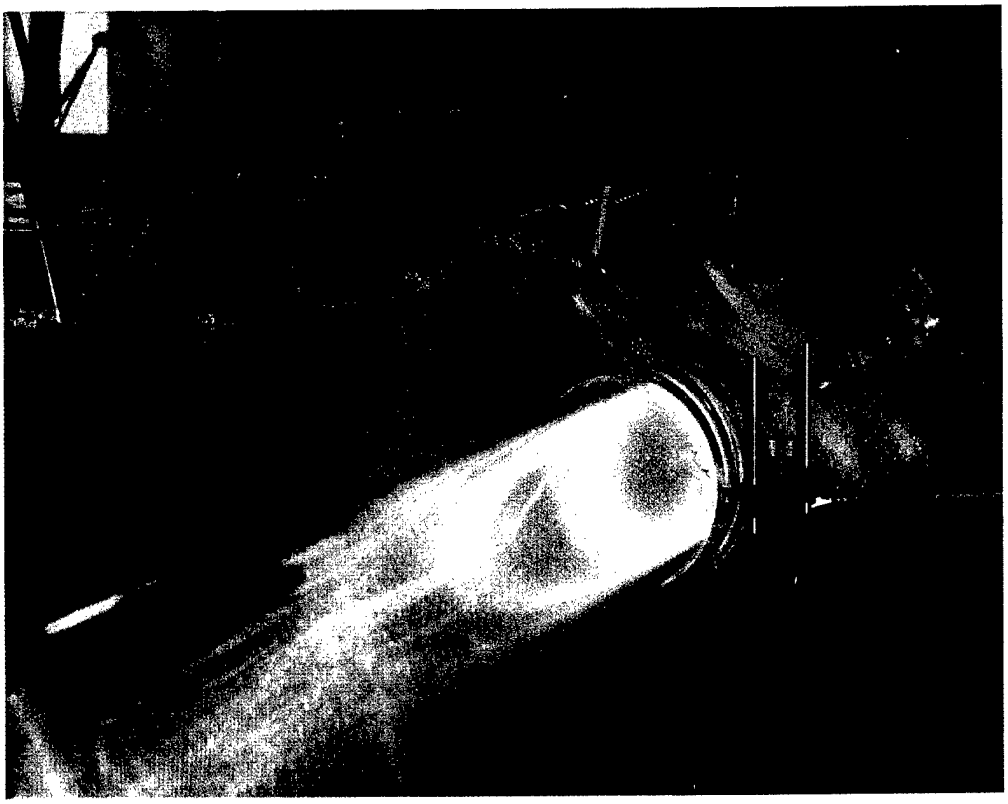

Fig. 18. Laser initiated-rf sustained argon plasma at 600 Torr at 2 kW. In a 10 cm diameter tube, the plasma density is 10^{12} /cc and volume is ~ 2500 cc. Note density is measured 10 cm away from the source region.

It can be seen in Fig. 19, that there is a considerable improvement over the comparable static argon discharges. The average plasma density is almost an order of magnitude higher. We attribute the higher density obtained for the laser initiated-RF sustained discharge to the following properties. The laser initiation will form a long plasma further away from the helical RF coil where the density is measured. This could allow the RF wave and power to sustain the ionization further from the coil than is the case when RF alone is used to obtain the plasma discharge [2,12,13].

We have also performed some initial experiments with N_2 as the background gas. Since TMAE is compatible with air over several minutes, this concept can also be extended to atmospheric air as the background gas. This experiment confirms that laser photo ionization of an organic seed gas is a viable method for initiating and sustaining a high-pressure discharge. It is also relevant to jet engine ignition at high altitude

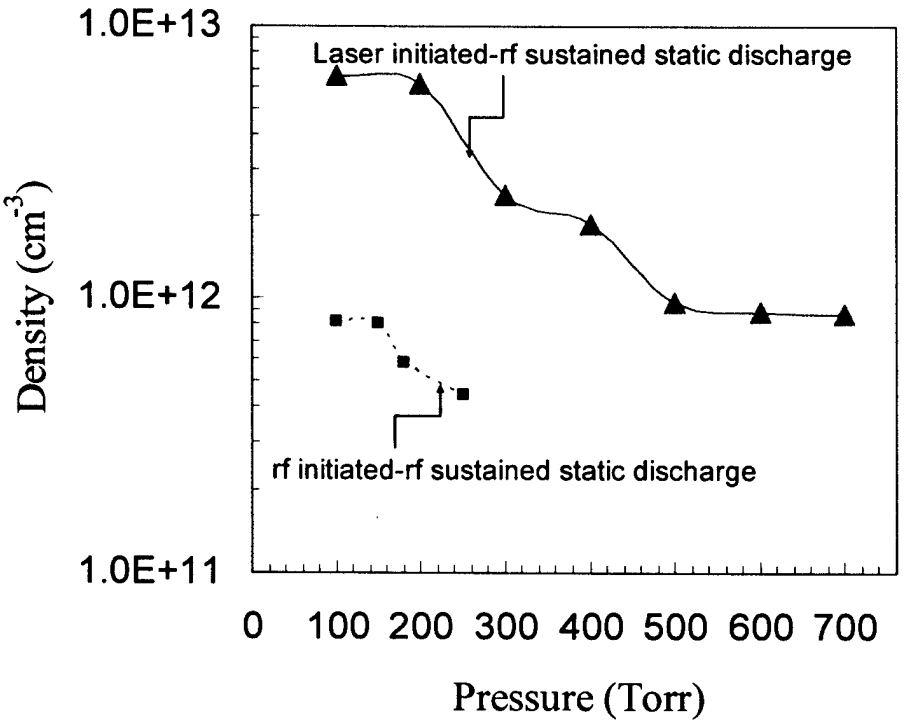

Fig.19. Comparison of laser initiated-RF sustained and RF initiated-RF sustained argon plasma density at modest RF power of 2 kW. Both mm wave amplitudes and phase shift data are used to obtain the plasma. Note density is measured 10 cm away from the antenna edge.

V. High Pressure Plasmas Produced by a Radio Frequency Plasma Source

High power (1-25 kW) radio frequency power sources have been installed and are being used to study the creation and sustainment of high-density plasmas of air constituents (Ar, N_2, O_2 and air) at high gas pressures. The skin depth for rf penetration is very short in these high-pressure plasmas and as a result such plasmas undergo strong radial and axial contraction being localized only under the antenna. The reduction in plasma volume makes this plasma unattractive for several applications. Discharges up to 10 Torr, sustained either by a dc or a high frequency source, fill the whole radial cross-section and these also have fairly large

axial extent [15-17]. However, as the gas pressure is increased further, at constant coupled rf power, the discharge becomes more and more contracted. In our experiment on radio-frequency inductively coupled plasma, in the pressure range below 10 Torr, a uniform plasma column filling the entire plasma chamber of length 150 cm and diameter 10 cm is obtained. However, as gas pressure is increased, initially the axial extent of the discharge decreases and then radial contraction occurs. Further increase in pressure results in a much contracted discharge right under the antenna with almost no axial extent. The gas flow rate along with the two- and three-body recombination rate has a strong influence on the characteristics of discharge contraction. The velocity of the gas fluid element is increased by increasing the flow rate. As a result, if the residence time of gas fluid element in the ionizing region under the antenna is smaller than the recombination time, a high-density air plasma may exist outside the antenna region. Alternatively, this can also be achieved if the effective recombination can be tailored to decrease by appropriate mixing of monoatomic gases to air constituents. Also small addition of Ar to a pure O_2 discharge, results in an increase of the positive ions and the reduction of electron attachment and hence negative ion [18].

The experiments exhibit a significant improvement in the plasma parameters namely, plasma density and plasma volume with the gas flow at comparable power levels. A high speed swirl injection flow on the periphery of the cylindrical chamber has been designed and utilized for this purpose. The role of the helical antenna configuration and grounding system along with the gas mix on the power coupled to the high density (10^{13}-10^{11} cm^{-3}) plasmas, have been investigated at high-pressure (1-250 Torr) of N_2, air and atmospheric pressure Ar. RF power is coupled to the plasma through a four or five-turn helical antenna, of length 13 cm and the internal diameter of 6 or 12 cm, using a redesigned capacitive matchbox system that allows more efficient RF coupling. In addition, we have also investigated the scaling of plasma parameters with the plasma chamber diameters of 10 cm and 5 cm.

A 105 GHz interferometer has been used to measure the plasma density and effective collision rate for highly collisional plasmas. The interferometer data is also used to estimate the effective recombination rate in high pressure plasma. Network analyzer measurements are made on the power coupling system to determine antenna impedance values. A photomultiplier tube and spectrometer are used to examine emission spectra, providing insight into the chemical (composition) and physical (temperature) processes in air constituent plasmas

A. Experimental System

The experimental set up is shown schematically in Fig.1. The plasma chamber is either a 5 or 10 cm diameter Pyrex glass tube of length 150 cm. The plasma chamber is pumped down to a base pressure of 1×10^{-6} Torr using a turbo molecular pump. Flow controllers and mixers are used to control the gas concentration. Two new pulsed, fixed frequency (13.56 MHz) radio frequency sources are employed to couple power. The first one is a 10 kW solid-state unit with variable duty cycle (90%-10%) and variable pulse repetition frequency (100 Hz-1 kHz) and very fast (μ sec) turn-on/off time. Another one is a 25 kW solid-state/triode unit with variable duty cycle and large (5 kW) fold back power.

The power is coupled through a helical antenna that excites the m=0 TE mode very efficiently. The helical antenna is 5 turns of quarter-inch copper tube of coil length 13.0 cm and internal diameter either 6 or 12 cm wound tightly over the plasma chamber. The end of the antenna is brought back to the capacitive match box to obtain a better ground and shielding. A new capacitive matching network has also been designed. As the losses in the antenna arise primarily from the connection points and solder joints, the antenna has been made out of a continuous length of copper tube, and the contacts were also modified. A high-speed swirl gas injection system has been designed to improve the gas flow system. In addition to an axial gas flow, four diagonally opposite holes, on either a 4 or 8 cm diameter circle (for 5 or 10 cm diameter chamber), tangentially inject the gas into the chamber. Swirl flow keeps the plasma off the inside walls of the chamber by creating a gas layer. This arrangement improves the thermal conductivity, reduces the excess heating of the plasma chamber and permits longer experimental runs without damaging the Pyrex chamber.

B. Gas Flow Effect

The effect of gas flow rate on axial plasma density and temperature profile away from the ionizing region has been studied. The velocity of a gas element in the discharge region increases with gas flow rate and as a result electrons are removed from the discharge region much faster than they are able to recombine. If electron residence time in the discharge region is much shorter than the time for electron-ion recombination, a high density plasma may exist

outside the ionizing region. If n_{e0} is the electron density in the ionizing region then electron density may decrease as the gas fluid element drifts out of the source region. The rate equation for this can be written as,

$$\frac{dn_e(z)}{dz} = -\frac{\alpha_{eff}}{u_m} n_e^2 \qquad (V.1)$$

Here α_{eff} is the effective recombination coefficient and u_m is the mean fluid drift velocity. If the drift velocity is assumed to be uniform over the cross-section of the element, then the electron density at distance z, from the ionizing zone is,

$$\frac{n_e(z)}{n_{e0}} = \frac{1}{1+\frac{\alpha_{eff} n_{e0} z}{u_m}} \qquad (V.2)$$

If the velocity of the fluid element is large such that $\alpha_{eff} n_{e0} z/u_m << 1$, then the plasma density decreases linearly with z.

$$n_e(z) \approx n_{e0}\left(1-\frac{\alpha_{eff} n_{e0} z}{u_m}\right) \qquad (V.3)$$

It can be concluded from the above equation that a high-density plasma may exist outside the ionizing region only if the residence time is much shorter than the recombination time. Since the recombination coefficient is much higher for diatomic ions, these may not survive outside the antenna region and therefore the density of these plasmas will be low outside the antenna region.

The mean velocity of the gas particle in the fluid element can be calculated using Bernoulli's equation. It can be easily shown that the flow rate of γ liters-per-minute (lpm) corresponds to $4\times10^{20}\ \gamma$ particles per second. If n_g is the gas density in the fluid element, then using the particle conservation, the mean velocity of the fluid element is

$u_m = 4\times10^{20}\frac{\gamma}{n_g A}$ cm/s, where A is the cross-sectional area in cm^2. The pressure balance equation for laminar flow is given by

$$n_g kT + \frac{1}{2}n_g a m_u v^2 = \eta L k T_r = 2.45\times10^{19}\zeta k T_r \qquad (V.4)$$

Here T and T_r are the gas and the room temperatures respectively, a is the atomic mass number and m_u the atomic mass unit, L is Loschmidt's number, k is the Boltzmann constant and ζ is the scaling factor (= Pressure (Torr)/760) that is unity at the atmospheric pressure. The mean velocity of the fluid element can be expressed as [19-20]

$$u_m = 32.64\frac{\gamma T}{A T_r\left(1+\sqrt{1-4\varepsilon}\right)\zeta} \text{ cm/s} \qquad (V.5)$$

where

$$\varepsilon = 5.13\times10^{-9} a\left(\frac{T}{T_r}\right)\left(\frac{\gamma}{\zeta A}\right)^2. \qquad (V.6)$$

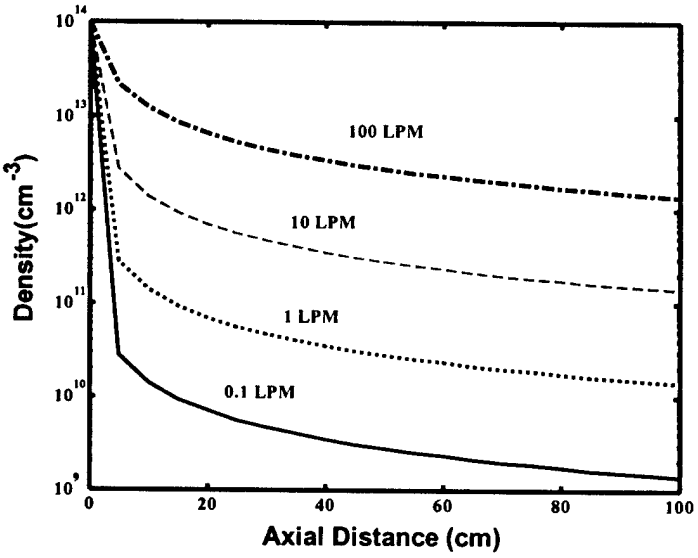

Fig. 20. Numerical plot of axial plasma density for 760 Torr of argon plasma at 5000 K at different gas flow rates with a recombination coefficient of $\alpha_r=10^{-11}$ cm^3/s.

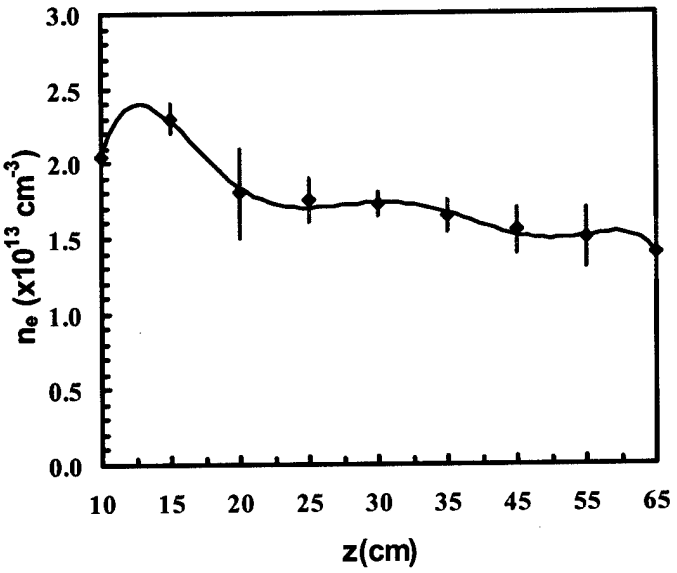

Fig. 21. Axial plasma density scan for atmospheric pressure argon vented to ambient air at 3.0 kW with flow rate of 20 lpm.

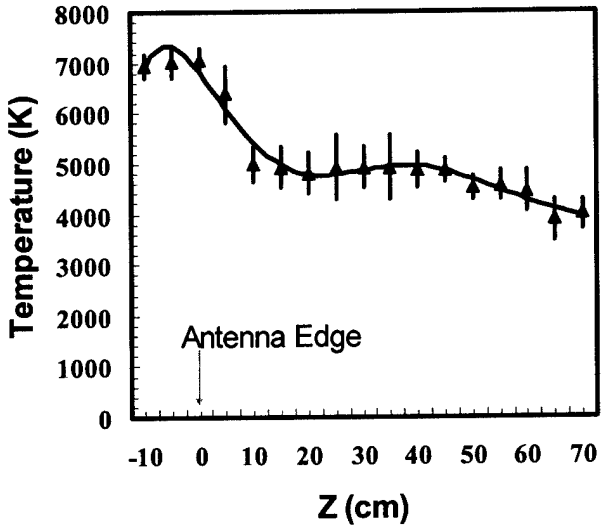

Fig. 22. Axial plasma temperature scan for atmospheric pressure argon vented to ambient air at 3.0 kW with flow rate of 20 lpm.

A numerical plot of axial plasma density for 760 Torr argon plasma with flow rate has been shown in Fig. 20 and the experimental results have been plotted in Fig. 21. The axial

plasma density decay away from the ionizing region is a strong function of the gas flow rate. It can be concluded that plasma projection outside the antenna region can be obtained at a high gas flow rate

The axial excitation temperature scan for the same plasma is shown in Fig. 22. An axially uniform, high-density plasma is produced with argon flow rate of 20 lpm in ambient air using a modest radio-frequency power of only 3.0 kW. In the static case (Figs. 24-26), plasma is localized under the antenna. In this situation, we obtain a lower density plasma (10^{12}/cc) of higher excitation temperature (~5000-7000 K).

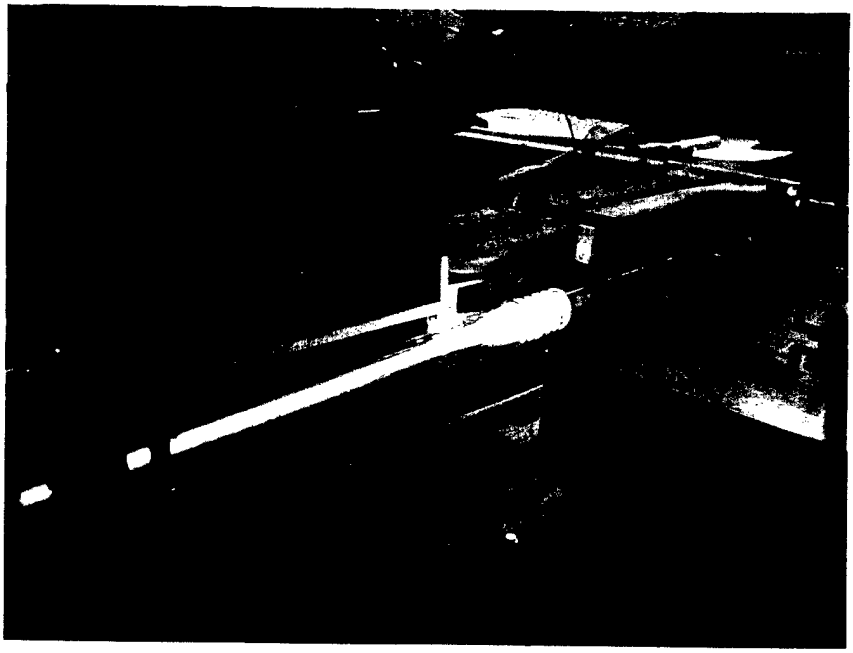

Fig. 23. Atmospheric pressure argon vented to ambient air at 3.0 kW with a flow rate of 20 lpm.

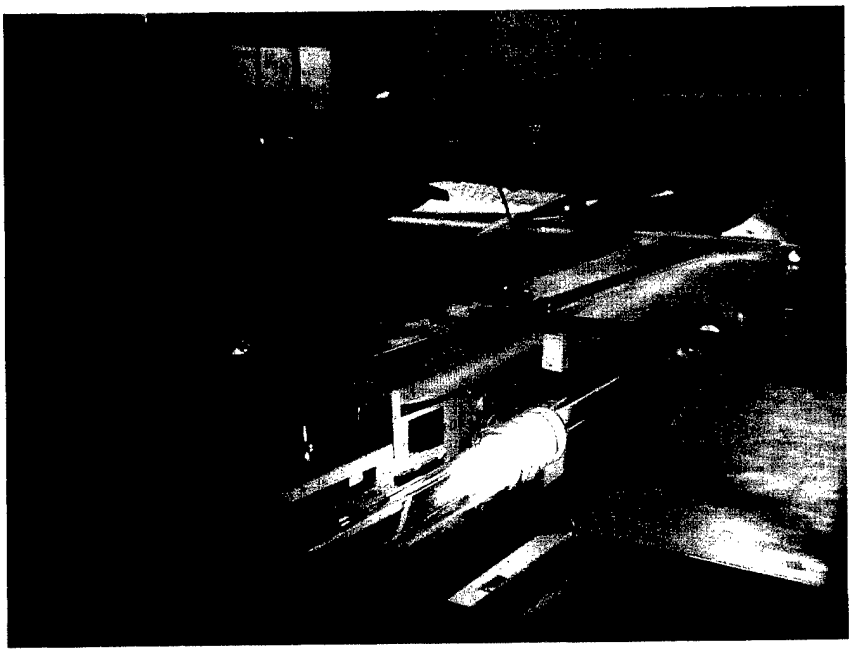

Fig. 24. Atmospheric pressure argon at 3.0 kW in static case.

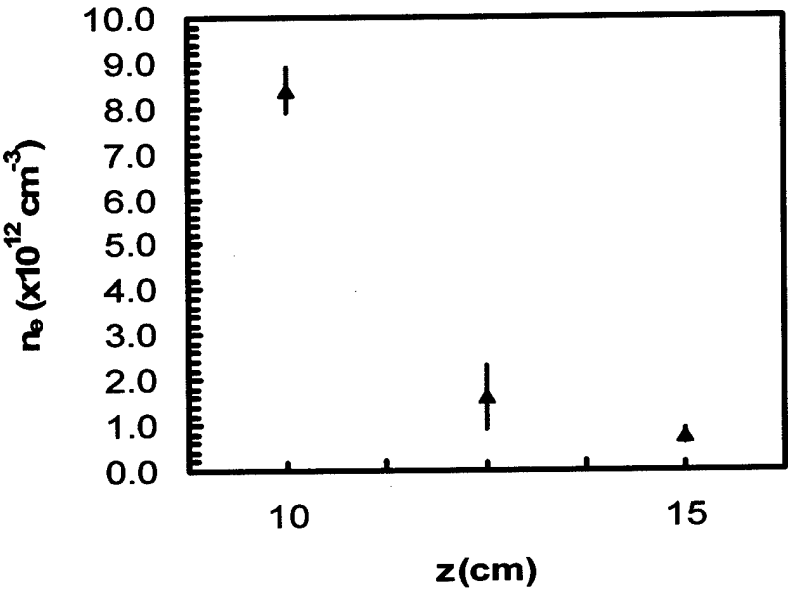

Fig. 25. Axial plasma density scan for atmospheric pressure argon at 3.0 kW in static case.

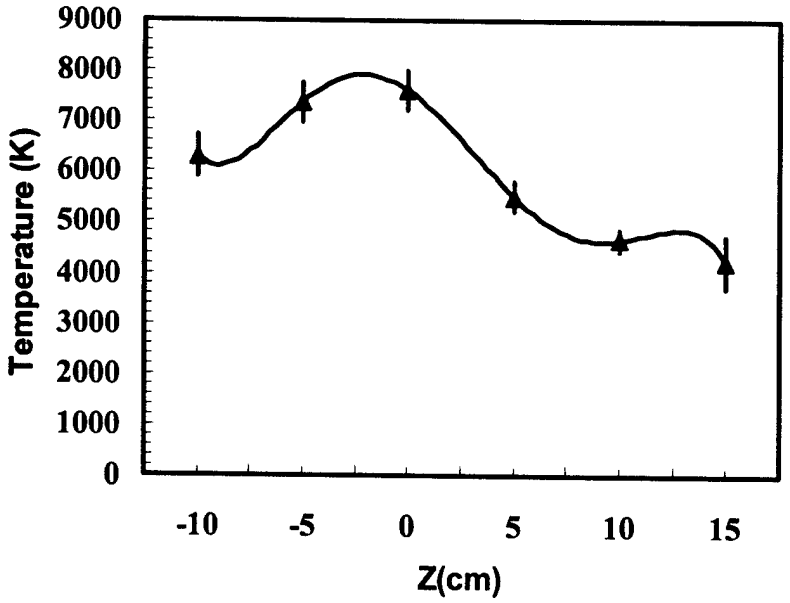

Fig. 26. Axial excitation temperature scan for atmospheric pressure argon at 3.0 kW in static case.

VI. A New Advance in the Application of 105 GHz millimeter Wave Interferometry for High Pressure, High Density Plasma Discharges.

We have used a 105 GHz quadrature interferometer and developed a new method of analysis for the first time, to our knowledge, to measure the plasma density and effective collision frequency in the presence of high collisionality due to high neutral gas pressures.

In the regime where collision frequency (ν) is of the order of the plasma (ω_p) and wave frequency (ω), the plasma density estimate using only phase data is inaccurate. Phase change corresponding to a given plasma density becomes much smaller in the presence of high collision frequency. Therefore, it is important to account for the high collisionality present at high gas pressures by including the amplitude change of the mm wave. The interferometer works by using an I-Q (In-phase and Quadrature phase) mixer to determine the phase and amplitude change of the 105 GHz mm wave signal going through the plasma. The I and Q

outputs are put into the X and Y inputs respectively of an oscilloscope to capture the data and then transfer that to computer through a VI control program (Fig 27). The interferometric plot shown in the Fig. 28, is used to determine the phase change as well as the signal attenuation. A numerical program in MATLAB solves for both phase and attenuation data to obtain the plasma density as well as the effective collision frequency. The density plot with time also reveals the loss mechanisms like effective recombination coefficients at higher gas pressure.

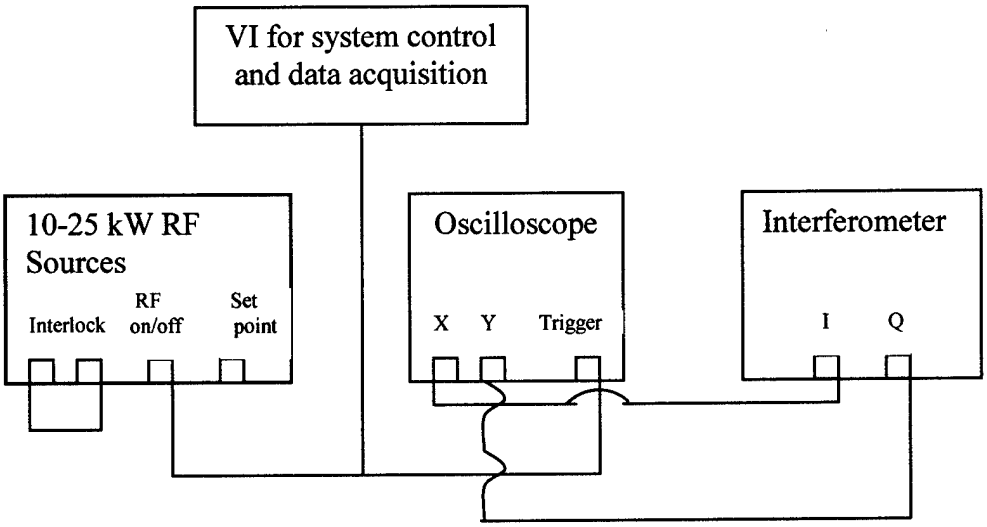

Fig. 27. Interferometer and data acquisition setup

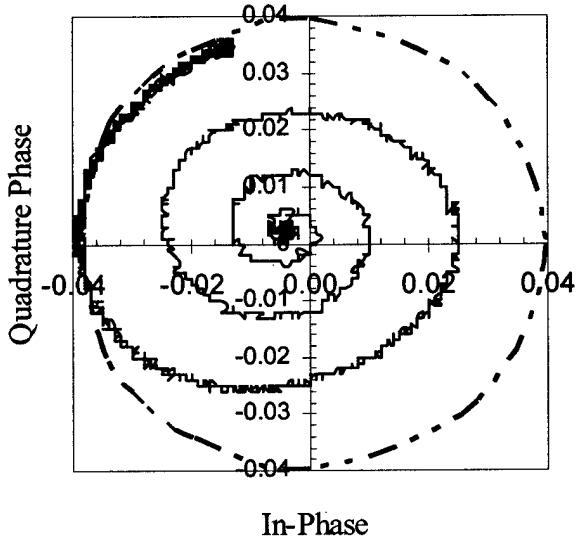

Fig. 28. Interferometer trace showing a nearly cut-off density of 9×10^{13} cm^{-3} in argon using a five turn Helical antenna. Measurements are made 10 cm away from the antenna

A. Theory

The complex dielectric constant for a linear medium is given by [4]

$$\kappa = \kappa_r + j\kappa_i = 1 - j\frac{\sigma}{\varepsilon_0 \omega} = 1 - \frac{\omega_p^2}{\omega^2 + \nu^2}\left(1 + j\frac{\nu}{\omega}\right) \qquad \text{(VI.1)}$$

Where σ is the complex Lorentz conductivity, ω_p the plasma frequency and ν is the effective collision frequency for momentum transfer, treated as viscous drag force. The complex refractive index is

$$\mu = \mu_r - j\chi = \kappa^{1/2}, \qquad \text{(VI.2)}$$

The complex propagation constant is written as

$$\gamma = \alpha + j\beta = \frac{\omega}{c}(j\mu) = \frac{\omega}{c}\sqrt{\kappa} \qquad \text{(VI.3)}$$

Here $\alpha = \chi\omega/c$ is the attenuation constant in Nps/m and $\beta = \mu_r\omega/c$ is the phase constant in rad/m.

The solution for the phase constant and attenuation constant yields,

$$\beta_p = \frac{\omega}{c}\left\{\frac{1}{2}\left(1 - \frac{\omega_p^2}{\omega^2 + \nu^2}\right) + \frac{1}{2}\left[\left(1 - \frac{\omega_p^2}{\omega^2 + \nu^2}\right)^2 + \left(\frac{\omega_p^2}{\omega^2 + \nu^2}\frac{\nu}{\omega}\right)^2\right]^{1/2}\right\}^{1/2} \qquad \text{(VI.4)}$$

$$\alpha_p = \frac{\omega}{c}\left\{-\frac{1}{2}\left(1 - \frac{\omega_p^2}{\omega^2 + \nu^2}\right) + \frac{1}{2}\left[\left(1 - \frac{\omega_p^2}{\omega^2 + \nu^2}\right)^2 + \left(\frac{\omega_p^2}{\omega^2 + \nu^2}\frac{\nu}{\omega}\right)^2\right]^{1/2}\right\}^{1/2} \qquad \text{(V.5)}$$

Assuming a plasma slab of uniform density profile, the total change in phase and amplitude for interferometric signal are given as

$$\Delta\varphi = \int_0^d (\beta_0 - \beta_p)dr \qquad \text{(VI.6)}$$

$$\Delta A = \int_0^d (\alpha_0 - \alpha_p) dr \qquad \text{(VI.7)}$$

Here β_0 and α_0 are the free space value and β_p and α_p are the plasma values. A numerical program in MATLAB is used to solve for plasma density and ν_{eff} simultaneously from experimentally measured $\Delta\phi$ and ΔA.

By simultaneously solving the phase change and attenuation data from the interferometer trace in time (Fig. 28), the plasma density as well as the effective collision frequency as a function of time can be also be estimated. The density decay plots also yield the effective recombination rate for the plasma at higher gas pressures.

The continuity equation, including the ambipolar diffusion term, the ionization frequency term ν_{iz} and two-body and three-body recombination term is given by,

$$\partial n_e/\partial t = D_n \nabla^2 n_e + \nu_{iz} n_e - \alpha_r n_e^2 - \beta_r n_g n_e^2 \qquad \text{(VI.8)}$$

Where, α_r, β_r and n_g are the two-body recombination rate, three-body recombination rate and the neutral gas pressure respectively. During the plasma decay in the absence of an ionizing source with high back ground gas pressure, the recombination losses dominate the diffusion loss. Therefore, one can write

$$\partial n_e/\partial t = -\alpha_r n_e^2 - \beta_r n_g n_e^2 \qquad \text{(VI.9)}$$

$$\partial n_e/\partial t = -(\alpha_r + \beta_r n_g) n_e^2 = -\alpha_{eff} n_e^2 \qquad \text{(VI.10)}$$

Here α_{eff} is the effective recombination term that includes two-body and three-body recombination effects. Thus the plasma density decay with time plot can be used to obtain α_{eff}.

The interferometeric trace for a 100 Torr argon plasma at 2 kW is shown in Fig 29. The post discharge trace is a function of time as plasma decays when the RF power is turned off. Each point on the trace corresponds to the instantaneous phase and amplitude change of the mm wave signal traveling through the plasma. The instantaneous plasma density and corresponding effective collision frequency are obtained by solving simultaneously the instantaneous phase and amplitude change data. The result is a Mat Lab plot of plasma density

and effective collision frequency as a function of time. A density decay plot is also obtained by taking the time derivative of density plot.

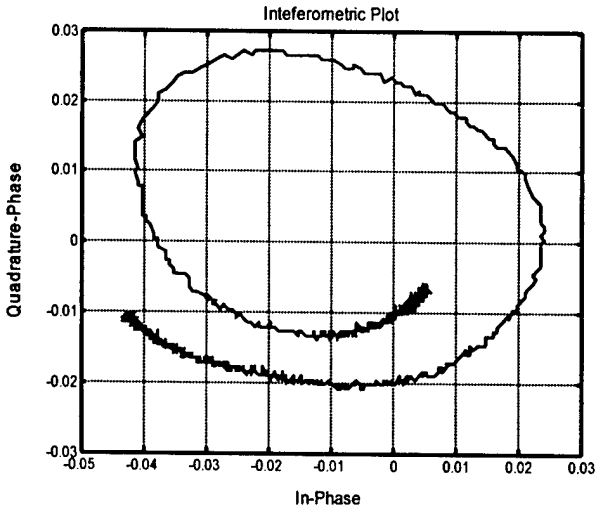

Figure 29. The interferometric trace for 100 Torr argon plasma at 2 kW. Each point corresponds to instantaneous plasma density and effective collision frequency.

It is seen that for constant plasma density, the effective collision frequency also remains constant. However, as the density starts to decrease, the effective collision frequency increases. The explanation for this effect lies in the thermal velocity (v) dependence of the collision frequency. As plasma decays, it also cools down in the process. Since for the dominant electron-neutral collisions, the collision frequency varies as $1/v$ and the cross-section varies as $1/v^2$, the collision frequency increases with plasma decay. The velocity dependence for electron-ion collision is even stronger as frequency dependence on velocity is $1/v^3$ and cross-section dependence is $1/v^4$ [4]. We observe that the effective collision frequency increases almost linearly as the plasma decays suggesting that the dominant collision mechanism here are electron-neutral collisions.

From the density decay plot, an estimate of the effective recombination coefficient is obtained using equation (VI.10). This provides an insight into the dominant loss mechanism present at high-gas pressure plasma. Thus this new analysis of interferometric data provides

and excellent measurement scheme for the plasma density in the presence of high collisionality due to high neutral gas pressures.

VII. Optical Emission Analysis of High Pressure Seeded Air Plasmas

A three channel Ocean Optics Spectrometer is used to capture the plasma spectral emission. The sample is acquired using fiber optic cables. The spectrometer output is connected to an A/D board in a PC. The data is acquired using a program written in Lab View. Each channel is a single grating spectrometer (1200 line/mm) which counts photons using a linear CCD array (2048 pixels). Samples are taken over the following ranges: 200-500 nm, 400-700 nm, and 600-850 nm. The three channel configuration allows for increased resolution over a single channel model designed for the same wavelength range. A new Lab View program has been developed and used in place of commercially available Ocean Optics software package. This program allows for correction of spectral attenuation of the fiber optics. This makes the results more accurate. Plasma spectral emission is used to study the chemical and physical processes in different gas mix plasma.

In diatomic gases like nitrogen/oxygen, a significant part of the RF power is consumed in exciting the rotational / vibrational energy states. This results in significant heating of the neutral gas without additional ionization. It is a significant drain of the energy source and leads to inefficient plasma production in air constituent gases. Therefore, an estimate of the neutral gas temperature becomes important. Since it is not possible to position the interferometer very close to the RF antenna due to possible arcing, the plasma characteristics in the source region can only be determined by the spectrometer. It is also used to correlate spectral density measurement with the 105 GHz interferometeric density results.

A. Spectroscopic Measurements:

The excitation and ionization process within an inductive discharge depends on the plasma temperature. If one assumes a Maxwellian electron energy distribution and partial local thermal equilibrium condition for the emitted lines, the plasma temperature can be estimated

using a Boltzmann plot. [21-24] In the presence of high collisionality present at higher gas pressures (> 10 Torr), the condition of partial local thermal equilibrium can be reasonably assumed. However, this leads to higher power consumption as the high-energy electrons are absent. The primary spectroscopic measurements that have been performed are the atomic excitation temperature T_{ex} and the molecular vibrational temperature T_{vib}. The atomic excitation temperature is obtained by measuring the emission intensities of the neutral atoms. In a Boltzmann plot for excitation, a set of spectral emission lines are chosen. For a given wavelength, the relative photon flux, I_{kj}, is determined from the spectral graph. Values of transition probability, A_k, oscillator strength, g_k, and the energy of the upper level, E_k, are obtained from the literature.[21]

In the absence of self-absorption, the relative photon flux for atomic emission is given by,

$$I_{kj} = \frac{Lhc\rho_0 A_k g_k}{4\pi\pi_{kj}} \exp\left(-\frac{E_k}{kT_{exi}}\right) \qquad \text{(VII.1)}$$

here h is the Planck's constant, k is the Boltzmann constant, c is the velocity of light, L is the path length, ρ_0 is the emission number density and T_{exi} is the excitation temperature.

Rearranging terms in Eq. (VII.1), we obtain,

$$\ln\left\{\frac{I_{kj}\lambda_{kj}}{g_k A_k}\right\} = \ln\left\{\frac{Lhc\rho_0}{4\pi}\right\} - \frac{E_k}{kT_{exi}}. \qquad \text{(VII.2)}$$

Thus the excitation temperature is obtained from inverse slope of ln $(I_k\lambda_k/g_kA_k)$ vs. E_k plot. However, it should be noted that the excitation temperature so obtained will not be equal to the kinetic temperatures of electrons and heavy species if the collisions are not frequent enough to bring about local thermal equilibrium (LTE).

In order to determine the vibrational temperature of nitrogen from the measured spectra, the following procedure is used. The spectral intensity of N_2 second positive band

$\left(C^3\Pi_u - B^3\Pi_g\right)$ of wavelengths 380.49, 375.44 and 371.05 nm are observed.[24-27] The choice of this band is for the following reason. In case of N_2, the lower end of the second positive band $B^3\Pi_g$ is about 20 electronic states above the lowest (ground) state $^1\Sigma_g^+$ and $B^3\Pi_g$ lies about 30,000 cm^{-1} below $C^3\Pi_u$. Since the bond length and strength in each electronic state is different, the moment of inertia and bond force constant of N_2 molecule in the B and C states are also different. This implies that the spacing of rotational levels and the vibrational levels in each electronic state will not be the same. The relative photon flux $I_{v'v''}$ for lines originating due to the transition of vibrational level (v', v'') is given by

$$I_{v'v''} \sim \bar{\nu}^4 \left|R_e^{v'v''}\right|^2 q_{v'v''} \exp\left(-\frac{G(v')hc}{kT_{vib}}\right) \qquad \text{(VII.3)}$$

The vibrational term value $G(v')$, the electronic transition probability $\left|R_e^{v'v''}\right|^2$ (the electron transition moment $R_e^{v'v''}$), and the Frank-Condon factor $q_{v'v''}$ for three lines are summarized in Table I. Thus the vibrational temperature is obtained from the inverse of slope of a straight line in a semi-logarithmic plot of

$$\ln\left[\frac{I_{v'v''}}{\bar{\nu}^4 \left|R_e^{v'v''}\right|^2 q_{v'v''}}\right] \text{vs. } G(v')hc \qquad \text{(VII.4)}$$

The following spectra were taken under steady-state conditions with a net power input of between 800-1200 W. Each spectral emission chart is the result of the average of three consecutive samples in order to increase the signal to noise ratio with a 150 ms integration time. Using a program written in Mat Lab, the emission spectrum is analyzed and excitation and vibrational temperatures calculated. The excitation temperature measurement presented in the last section.

Table I: Spectroscopic parameters of three vibrational nitrogen lines.

(v', v'')	Wavelength(nm)	G(v') (cm^{-1})	$\left\|R_e^{v'v''}\right\|^2$	$q_{v'v''}$
(0,2)	380.49	1016.474	456.4	0.14691
(1,3)	375.44	3006.754	461.7	0.20027
(2,4)	371.05	4940.144	467.9	0.16138

Figure 31 shows the spectral emission for pure argon and nitrogen respectively at a gas pressure of 600 Torr and 30 Torr. Figures 21 and 22 show spectral emission for nitrogen-argon mixes at 20 and 40 Torr respectively. As can be seen in Fig. 16, argon has intense emission lines in the 700-800 nm wavelength range whereas pure nitrogen has intense lines in the 300-400 nm wavelength range and a series of broader peaks in the 500-800 nm wavelength range (Fig. 32). These nitrogen lines in the 300-400 nm wavelengths are related to vibrational states of the nitrogen. Relative changes in the intensity of these peaks when both gases are present give an indication of any seed gas effects that are present.

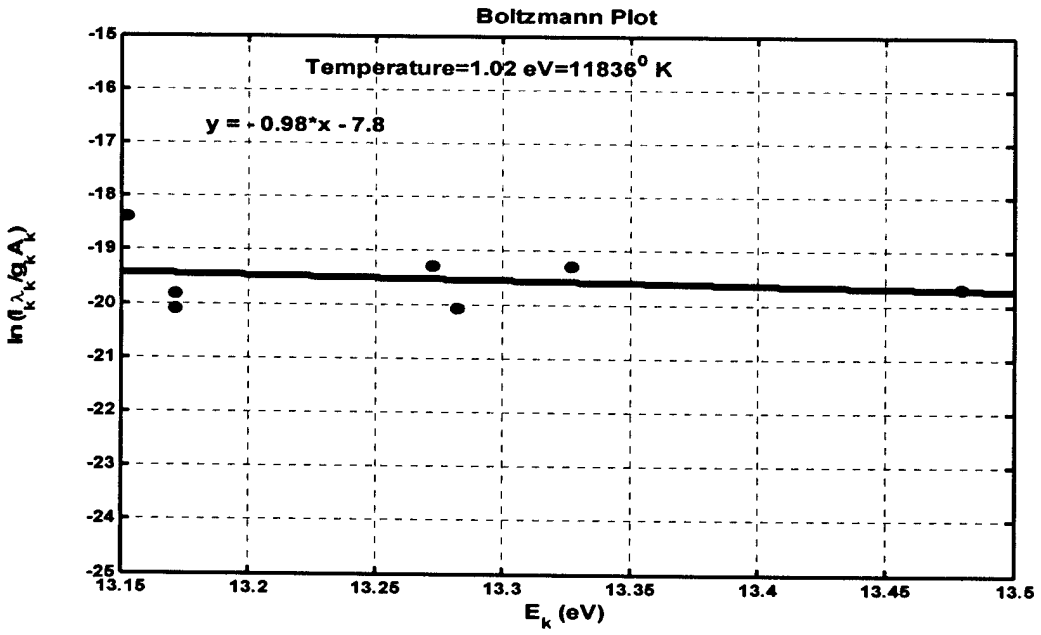

Fig. 30. A typical Boltzmann plot for Ar emission under the antenna for flow case.

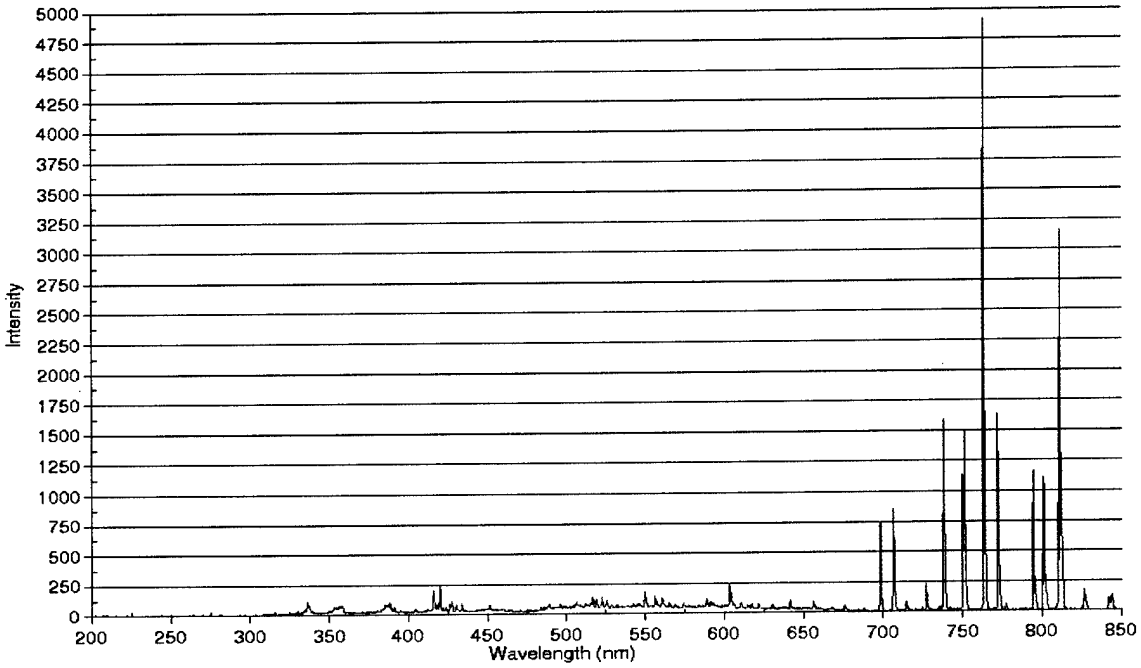

Fig. 31. Spectral emissions of argon plasma at 600 Torr.

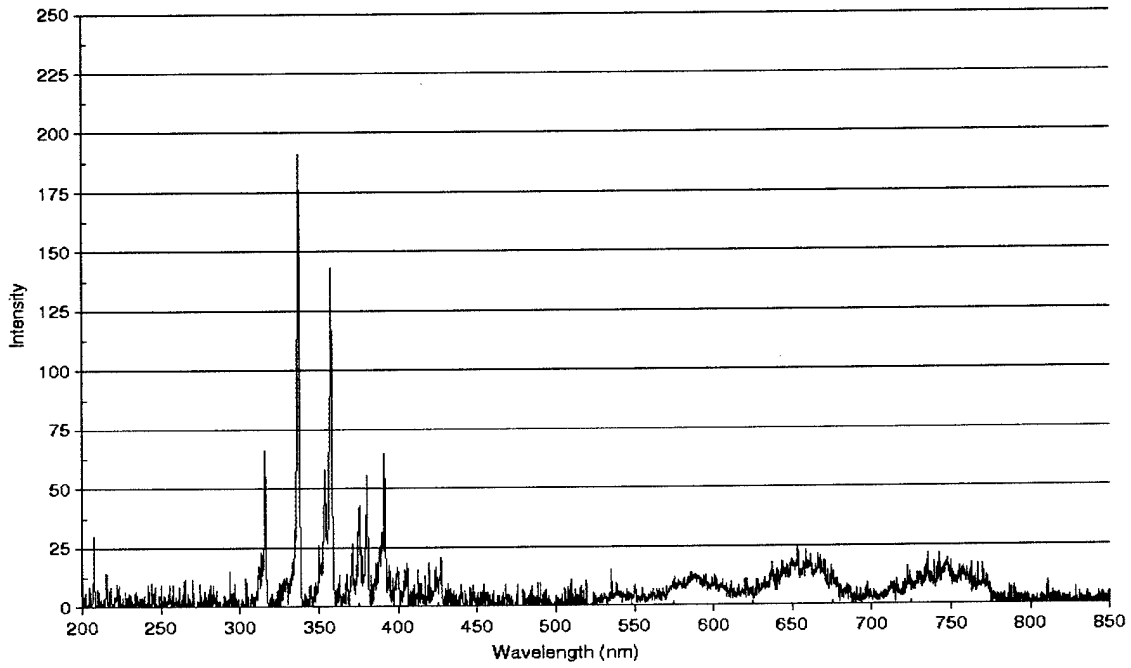

Fig. 32. Spectral emission of nitrogen plasma at 30 Torr.

VIII. RF Wave Penetration in Collisional Plasmas with a DC Magnetic Field

Helicon plasma source experimental and modeling research has been carried out by our research group [26]. We have measured wave magnetic field penetration into the plasma in the presence of magnetic fields. We have also used wave field measurements to model the corresponding electron energy distribution function and found evidence for non-Maxwellian distributions that can enhance the ionization efficiency of the source when compared to an equilibrium Maxwellian distribution. To examine the effects of plasma density, RF frequency, collisionality and DC magnetic field effects on RF plasma penetration on our University of Wisconsin facility, we carried out initial experiments on our double-half-turn helix helicon source. Figure 33 shows the experimental facility. Projection of plasmas well away from the source region (1 m) at high pressure and collisionality is an important feature for air plasmas. The RF wave penetration away from the antenna source region is a key issue for highly collisional plasma production. Theoretical research by Bozeman and Hooke [27], Weibel [28], and Godyak [29] has shown that DC magnetic field, high plasma density and nonlinear wave effects can enhance RF penetration in collisional plasmas. Our facility has a miniature electrostatically shielded, hybrid combiner (-35 dB common mode rejection) RF magnetic field probe that can measure wave axial penetration for a wide range of collisional plasma parameters. We illustrate our initial RF penetration results as the wave power, plasma density and magnetic field are increased.

Experiments have been conducted on our helicon source to investigate wave penetration in various operating modes, particularly under different DC magnetic field strengths. Wave penetration and uniformity away from the antenna region is crucial for a variety of applications, notably materials processing. Our facility has a number of diagnostics to investigate these phenomena, including a Langmuir probe and an enclosed wave magnetic field probe, as well has millimeter wave interferometry. Argon plasmas are produced at 3 mTorr with DC magnetic fields ranging from 200 to 1000 G, with 13.56 MHz RF input power into a half-turn double-helix antenna at up to 1 kW of pulsed power. Computational modeling, including the ANTENA and MAXEB codes, supplement the experimental results. The facility is illustrated in Fig. 33.

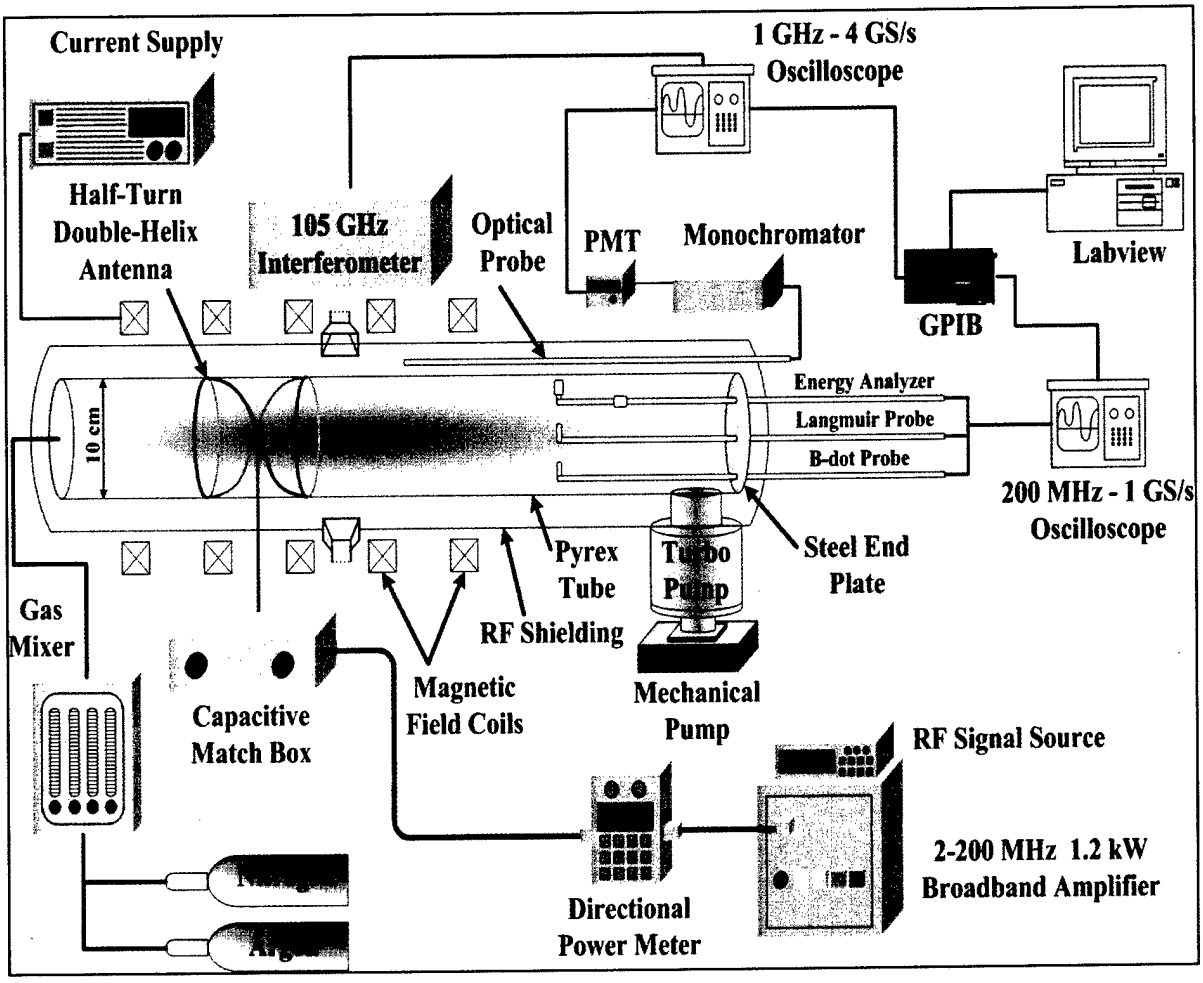

Fig. 33. Schematic diagram of the RF wave penetration facility

A calibrated wave magnetic field probe is used to measure RF penetration into the plasma, and is phase referenced to a second probe that measures the wave phases at the antenna input. It consists of a small (2 mm diameter) 5-turn loop enclosed in Pyrex. The output of the magnetic field probe is sent through a hybrid combiner to suppress (-35 dB common mode rejection) electrostatic pickup. Data for the z (axial) component of the wave B-field is presented for two coupling modes, the "transition" mode (200 G) and the "helicon" mode (1000 G) with an input power of 800 W in argon at 3 mTorr. Data is taken 1.5 ms into the RF pulse, where the helicon plasma is in quasi-steady-state. Amplitudes are presented in normalized units for comparison.

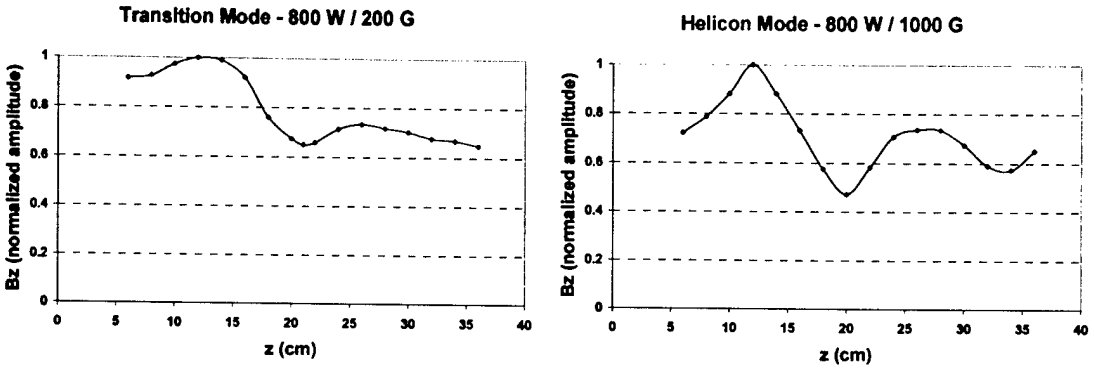

Fig. 34. Wave Bz magnitudes for Transition and Helicon Mode

Both modes exhibit significant axial wave penetration away from the antenna region (z = 0 cm is the edge of the antenna) compared to the case in which no DC magnetic field is present. The densities are $4x10^{12}$ cm^{-3} for the transition mode and $3x10^{13}$ cm^{-3} for the helicon mode. We see that despite the higher density and collisionality for the helicon regime, the helicon case with the increased magnetic field shows slightly enhanced wave penetration to that of the lower magnetic field transition case.

Computational results are quite similar to the experimental data. The following are results of AntenaII [Mouzouris and Scharer96] code runs whose input parameters closely correspond to the above transition and helicon mode cases. Input parameters account for the increased density and collisionality for the helicon case. The modeling is for a plasma column of greater length than the experimental apparatus to better illustrate the extent of wave penetration. Again, the end edge of the antenna is at z = 0 cm. A linear curve fit is added to show the average overall wave attenuation along the axis.

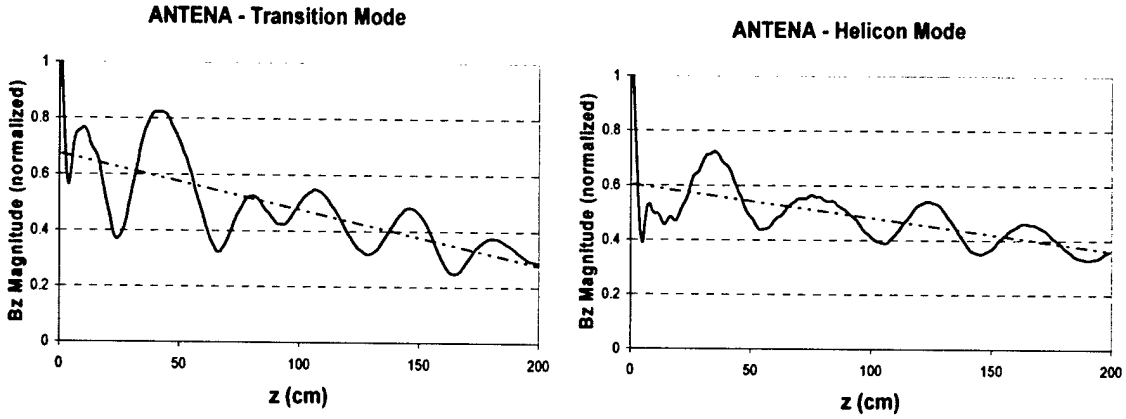

Fig. 35. ANTENA code results

In both cases the wave penetrates far into the plasma, well away from the antenna compared to the no magnetic field inductive case. The axial attenuation is slightly less in the case of the helicon mode, despite the higher density (10^{13} cm^{-3} versus 2.3 x 10^{12} for the transition mode) and collision frequency, further illustrating the enhancement of wave penetration with increasing magnetic field.

Further ANTENA modeling results for a high-density 3×10^{13} cm^{-3}, 300 mTorr collisional ($\nu=8\times10^{8}$ s^{-1}) plasma also show enhanced axial skin depth penetration (1/e) due to an increase in the magnetic field for different frequencies.

The full antenna k-spectrum and radial plasma profiles are included in the model that indicates greater skin depth penetration with increasing static magnetic field and lower frequency.

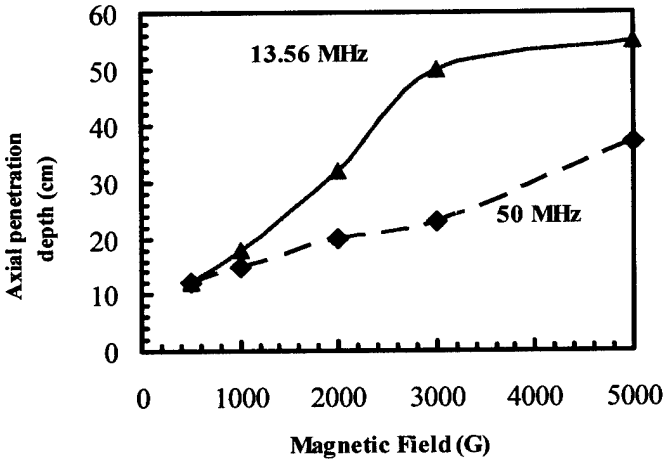

Fig. 36. Axial penetration depths vs. magnetic field profile for two rf frequencies

Both Langmuir probe and 105 GHz millimeter wave interferometry are used to measure the plasma density. Density profile effects and the influence of collisionality at high densities are included in the data analysis. Densities over a range of magnetic fields for constant input power are presented below, obtained by both methods. Note the close correlation between these result.

The results show that increasing the applied DC magnetic field produces higher densities over the range of magnetic fields we are able to produce. The moveable Langmuir

probe can also measure the axial density profile over the 6 ms RF pulse. Measurements are taken at a radius of 2.5 cm. Spatio-temporal results for four cases are presented below.

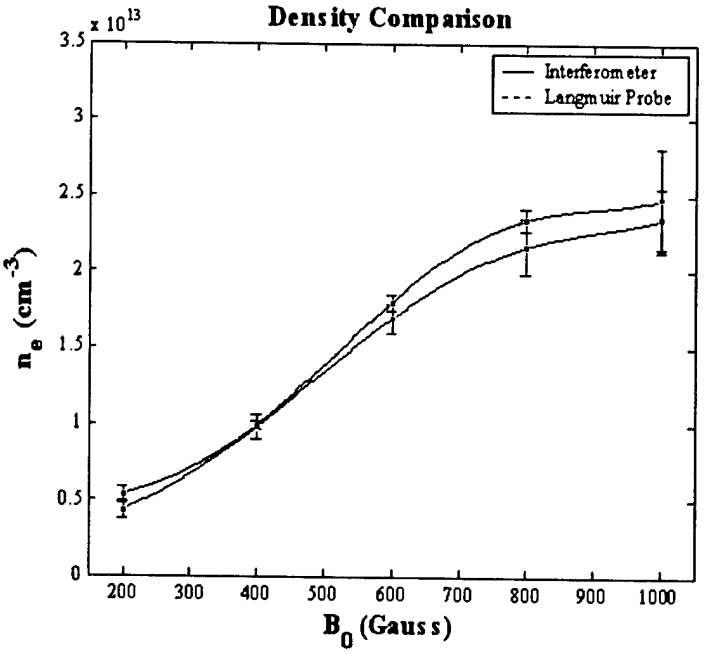

Fig. 37 Density vs. DC magnetic field using Langmuir probe and interferometer

Clearly the extension of the plasma density away from the antenna is a function of both the power input and the DC magnetic field. For the inductively coupled case (a) (600 W/200 G) the density is confined to the region closest to the antenna. As the power is increased to 800 W (b) in the transition to helicon coupling, the density begins to extend axially, peaking away from the antenna. As the magnetic field is increased to 600 G (c) and 1000 G (d), helicon propagation occurs and the effect becomes even more pronounced. The greatest penetration and uniformity occurs for the highest magnetic field, the 1000 G case. Also note that the helicon cases sustain density during the duration of the pulse better than those with lower magnetic fields.

We will continue to investigate the role of DC magnetic fields and input powers in wave penetration for high pressure air plasmas. We will examine additional electromagnets to extend the axial length of the magnetic field and power supplies to increase the magnetic field.

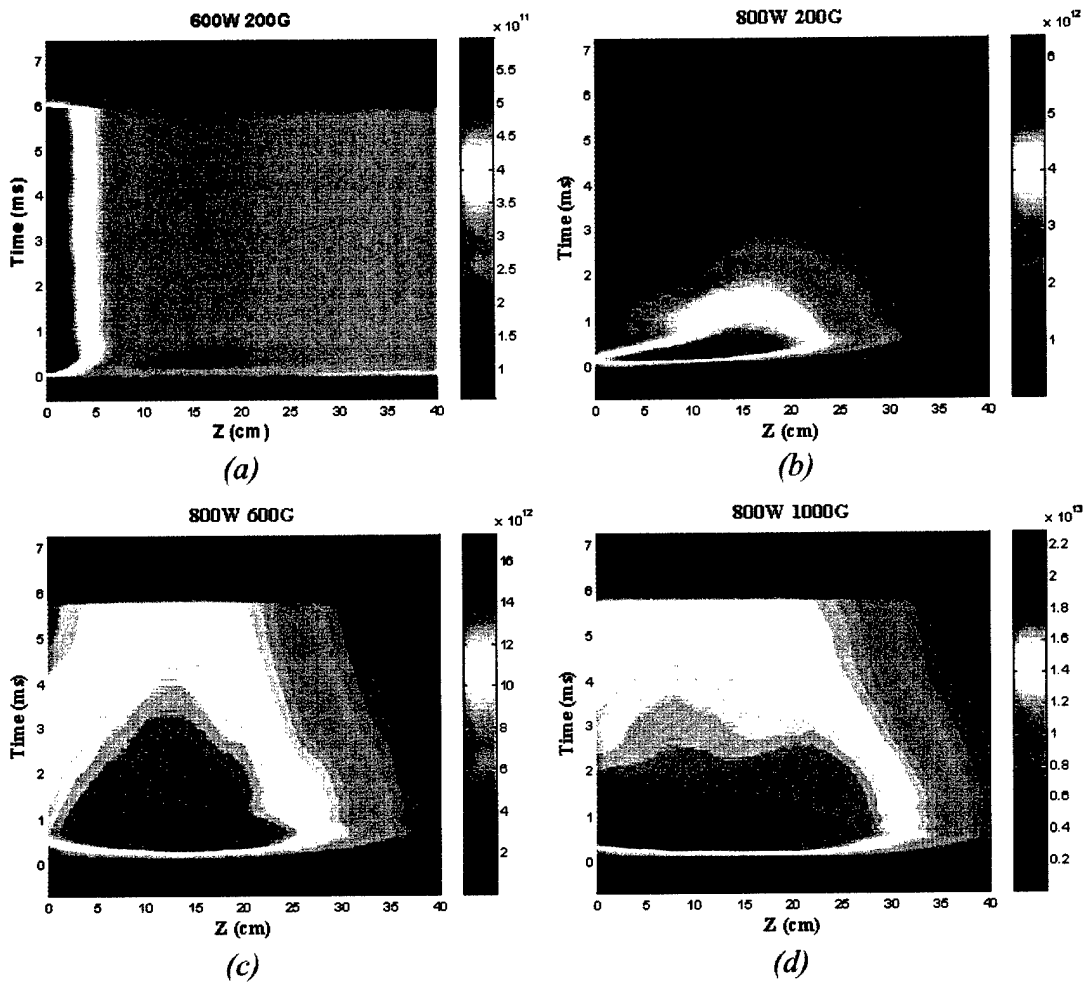

Fig. 38. Spatio-temporal plots of density for inductive coupling (a), the transition to helicon operation (b), and full helicon propagation (c and d)

IX. Contributions to a new book on Non-Equilibrium Air Plasmas

We met with the editors, other chapter masters and contributors in January, 2003 at Stevens Institute of Technology and worked out the contents of the Chapter on High Frequency Plasmas for which Professor Scharer will serve as chapter master. Ten contributors from six institutions have been contacted and have agreed to contribute to various sections of the chapter for the book. Our research group has also agreed to contribute a section on mm wave interferometry in high density, highly collisional plasmas in the section on plasma diagnostics for the book. The outline for the chapter is as follows:

Chapter 7- High Frequency Air Plasma Sources

7.1 Introduction and Overview (J. Scharer)

7.2 Laser initiated or sustained, seeded high pressure plasmas (W. Rich, I. Adamovitch, K. Akhtar, W. Lempert, J. Scharer)

A. Seed gas injection

1. CO (OSU)

2. TMAE (UW)

B. Laser or flashtube ionization and excitation

1. CO laser (OSU)

2. UV laser (UW)

7.3 Radio-frequency and Microwave sustained high pressure plasmas (S. Kuo, C. Laux, C. Kruger, K. Akhtar, J. Scharer)

A. Radiofrequency (RF) and Microwave Ionization and Sustainment (C. Laux, C. Kruger, K. Akhtar, J. Scharer)

(Ionization and breakdown, use of seed gas ionization and gas flow to reduce sustainment power, dominant loss mechanisms (rotational, vibrational) and metastable states, rf penetration with frequency and magnetic field effects).

1. Review of RF Plasma Torch and Stanford Experiments (C. Laux, C. Kruger,)

2. Wisconsin Laser Initiated and RF Sustained experiments (J. Scharer, K. Akhtar)

3. Microwave ionization and sustainment (S. Kuo, J. Scharer, K. Akhtar, (review literature and note differences with RF cases)

7.4 E-beam produced high pressure plasmas, (C. Laux, C. Kruger, W. Rich, R. Vidmar)

A. OSU Electron-Beam experiment with laser excitation. Electron-beam formed plasmas and window (Beam voltage and power, window technology issues, spatial penetration, power requirements) (W. Rich, I. Adamovitch, W. Lempert, R. Vidmar)

B. Stanford Short Pulse Experiment in an RF Torch Produced Plasma (C. Kruger, C. Laux)

We will edit and make contributions to the book that will be completed in the fall, 2003.

X. References

1. G. Ding, J. E. Scharer, K. Kelly, "Diagnostics and Analysis of Decay Process in Laser Produced Tetrakis (dimethyl-amino) Ethylene Plasma," Physics of Plasmas, Vol. 8, No. 1. January (2001) pp 334-342.

2. Kamran Akhtar, John Scharer, Shane Tysk, and Mark Denning, " Radio-Frequency Sutainment of Laser Initiated, High-Pressure Air Constituent Plasmas", 15th Topical conference on Radio Frequency Power in Plasmas, Jackson Lake Lodge, Grand Teton National Park, Moran, Wyoming, May19-21, 2003.(To be published in AIP Conference Proceedings)

3. K. Akhtar, J. Scharer, S. Tysk, and E. Kho, Rev. Sci. Instrum., **74**, 996 (2003).

4. C. B. Wharton, "Plasma Diagnostics Technique", Ed. R.H. Huddelstone and S.L. Leonard, Academic Press, New York, 1965.

5. K. L. Kelly, J.E. Scharer, E.S. Paller, and G. Ding, "Laser Ionization and Radiofrequency Sustainment of High-Pressure Seeded Plasmas", Jour. of Applied Physics, Vol. 92, No. 2, July (2002) pp 698-709.

6. Y.P. Raizer, in *Gas Discharge Physics*, (Springer-Verlag, Berlin Heidelberg, 1991), pp 62.

7. M.Capitelli, C.M. Ferreira, B.F. Gordiets and A.I. Osipove, *Plasma* Kinetics in Atmospheric Gases, (Springer Verlag, Berlin, 2000) pp140.

8. D.R. Bates, J. Phys. B., **13**, 2587 (1980).

9. R.A. Holroyd, J.M. Preses, and C.L. Wody, Nucl. Instr. And Meth. Phys. Res., A261, 440, (1987).

10. L.M. Biberman, V.S. Vorob'ev, and I.T. Yakubov, in Kinetcis of Nonequilibrium Low-Tempearture Plasmas, Consultant Bureau, NewYork, 1987,p412.

11. S.Toby, P.A. Astheimer and F.S. Toby, J.Photochem. Photobiol. A: Che., 67, 1 (1992)

12. J. Scharer, K. Akhtar, K. Kelly, B. White, S. Tysk, "Laser Initiation and Radiofrequency Sustainment of Seeded High Pressure Plasmas", P 92, IEEE Catalog 02CH37340, P29th IEEE International Conference on Plasma Science, May 26-30, 2002, Banff, Alberta, Canada (Invited talk).

13. Kamran Akhtar, John E. Scharer, Kurt L. Kelly, Shane Tysk and Ben White "Radio Frequency Sustainment of Laser Initiated Seeded High-Pressure Discharge." P 149, IEEE Catalog 02CH37340, 29th IEEE International Conference on Plasma Science, May 26-30, 2002, Banff, Alberta, Canada.

14. Ben White, Kamran Akhtar Shane Tysk, John E. Scharer and Eric S. Paller, " Radio Frequency Produced High-Pressure Air Constituent Plasmas", P 149, IEEE Catalog 02CH37340, 29th IEEE International Conference on Plasma Science, May 26-30, 2002, Banff, Alberta, Canada.

15. J.T. Massey and S.M. Cannon, J.Appl. Phys. 36,361(1965).

16. J.T.Massey, J.Appl. Phys. 36,373(1965).

17. Y Kabuzzi, M.D. Calzada, M.Mosian, K.C.Tran, and C.Trassey , J.Applied Phys., 91, 3, 1008, 2002.

18. C. Lee and M.A. Leiberman, JVST A, 13(2), 368, (1995).

19. H. S. Uhm and S. H. Song, Combust. Sci. Technol. **152**, 147 (2000).

20. S.Y. Moon, W. Choe, H .S.Uhm, Y. S. Hwang and J.J. Choi, Phys. Plasmas, 9, 4045, (2002).

21. R.H.Tourin, "Spectroscopic Gas Temperature Measurement", Elsevier Publishing Company, Amsterdam, 1966.

22. G. Herzberg, "Molecular Spectra and Molecular Structure Spectra of Diatomic Molecules", Van Nostrand Reinhold Company, New York, 1950.

23. N. Hamamoto, H. Kawazoe, Y. Nakmura, N. Arai, and K. Kitagawa, Energy Conversation and Management, Vol. 38, No. 10, 1177, 1996.

24. H.J. Eckert, F. L. Kelly and H. N. Olsen, "Spectroscopic Observation on Induction-Coupled Plasma Flames in Air and Argon," J. Applied Physics, Vol. 39(3), 1968.

25. National Institute of Standards and Technology, NIST Atomic Spectra Database, NIST Standard Reference Database#78.

26. J. Scharer, A. Degeling, G. Borg, and R. Boswell, "Optical Measurements and Analysis of Fast Electron Effects in Helicon Plasma Source," Physics of Plasmas 9, 3734-3742 (2002).

27. S.P Bozeman and W.M. Hooke, Plasma Sources Science and Technology, Vol. 3, pp. 99-107, (1994).

28. E.S. Weibel E.S., Phys. Fluids, 10, 741, (1967).

29. V.A. Godyak and R.B. Piejak, J. Appl. Phys., 82, 5994 (1997)

XI. Journal Publications (May, 2000 - May, 2003)

1. Kamran Akhtar, John E. Scharer, Shane M. Tysk and Enny Kho, "Plasma Interferometry at high pressures", Rev. Sci. Instrum., **74**, 996-1001 (2003).

2. J. Scharer, A. Degeling, G. Borg, and R. Boswell, "Optical Measurements and Analysis of Fast Electron Effects in Helicon Plasma Source," Physics of Plasmas 9, 3734-3742 (2002).

3. K.L. Kelly, J. E. Scharer, E. S. Paller, and G. Ding, "Laser Ionization and Radiofrequency Sustainment of High-Pressure Seeded Plasmas," Jour. Of Applied Physics 92, 696-709 (2002).

4. G. Ding, J.E. Scharer, K. Kelly, "Diagnostics and Analysis of Decay Process in Laser Produced Tetrakis (dimetlyl-amino) Ethylene Plasma," Physics of Plasmas, Volume 8, No. 1, 334-342, January (2001) http://ojps.aip.org/pop/

5. E. Paller, J. Scharer, K. Akhtar, K. Kelly and G. Ding, "Radiofrequency Initiation and Radiofrequency Sustainment of Laser Initiated Seeded High Pressure Plasmas" pp 526-529, Radio Frequency Power in Plasmas, 14th topical conference, AIP Conference Proceedings-595, Oxnard, CA May 2001.
http://ojps.aip.org/proceedings/plasma_phys.jsp.

Invited Talk: Prof. Scharer delivered an invited talk at ICOPS 2002.

J. Scharer, K. Akhtar, K. Kelly, B. White, S. Tysk, "Laser Initiation and Radiofrequency Sustainment of Seeded High Pressure Plasmas", P 92, IEEE Catalog 02CH37340, P29th IEEE International Conference on Plasma Science, May 26-30, 2002, Banff, Alberta, Canada.

XII. Conference Papers: (May, 2000 - May, 2003)

1. Kamran Akhtar, John Scharer, Shane Tysk, and Mark Denning, " Radio-Frequency Sutainment of Laser Initiated, High-Pressure Air Constituent Plasmas", 15th topical conference on Radio Frequency Power in Plasmas, May19-21, 2003, Jackson Lake Lodge, Grand Teton National Park, Moran, Wyoming.

2. Kamran Akhtar, John E. Scharer, Shane Tysk, Ben White, C. Mark Denning and Enny Kho," High-Pressure Air Constituent Plasmas", 55th Annual Gaseous Electronics Conference, October 15-18, 2002, University of Minnesota, Minneapolis, Minnesota, USA.

3. John E. Scharer, Ben White, Shane Tysk, Kamran Akhtar and Mark Denning, " Optical and Magnetic Field Measurements for a Helicon Source with Axial Density Gradients", Bulletin of the American Physical Society, Division of Plasma Physics Meetings, Volume 46, No. 8, November 11-15 2002, p. 62, Orlando, Florida, USA.

http://www.aps.org/meet/DPP01/baps/tocC.html Conf. Record CM1.0

4. J. Scharer, K. Akhtar, E. Paller, B. White, S. Tysk, "Optical Diagnostic for Examination of Fast and Thermal Electrons from a Helicon Plasma Source", P 166, IEEE Catalog 02CH37340, P29th IEEE International Conference on Plasma Science, May 26-30, 2002, Banff, Alberta, Canada.

5. Kamran Akhtar, John E. Scharer, Kurt L. Kelly, Shane Tysk and Ben White "Radio Frequency Sustainment of Laser Initiated Seeded High-Pressure Discharge." P 149, IEEE Catalog 02CH37340, 29th IEEE International Conference on Plasma Science, May 26-30, 2002, Banff, Alberta, Canada.

6. Ben White, Kamran Akhtar Shane Tysk, John E. Scharer and Eric S. Paller, " Radio Frequency Produced High-Pressure Air Constituent Plasmas", P 149, IEEE Catalog 02CH37340, 29th IEEE International Conference on Plasma Science, May 26-30, 2002, Banff, Alberta, Canada.

7. Shane Tysk, John Scharer, Kamran Akhtar, and Ben White, "Electron Energy Distribution Function in a Helicon Discharge", P 224, IEEE Catalog 02CH37340, 29th IEEE International Conference on Plasma Science, May 26-30, 2002, Banff, Alberta, Canada.

8. J. Scharer, B. White, S. Tysk, E. Paller and K. Akhtar, "Optical Emission, Electron Energy, Density, Wave Magnetic Field and Spectrum Measurements in a Helicon Plasma Source", P 225, IEEE Catalog 02CH37340, 29th IEEE International Conference on Plasma Science, May 26-30, 2002, Banff, Alberta, Canada.

9. Kamran Akhtar, John Scharer, Eric Paller, Ben White and Shane Tysk," Radio frequency Produced Air Constituent Plasmas", 43rdAnnual Meeting of the Division of Plasma Physics, American Physical Society, October 29 - November 2, 2001, Long Beach, California, USA. Bulletin of the American Physical Society, Division of Plasma Physics Meetings, Volume 46, No. 8, October 2001, page 63. CM1.029 http://www.aps.org/meet/DPP01/baps/tocC.html

10. Eric Paller, John Scharer, Kamran Akhtar, Rong Cao, Shane Tysk and Ben White, "Measurements and Analysis of Electron Distribution and Ionization", 43rdAnnual Meeting of the Division of Plasma Physics, American Physical Society, October 29 - November 2, 2001, Long Beach, California, USA. Bulletin of the American Physical Society, Division of Plasma Physics Meetings, Volume 46, No. 8, October2001, p62. CM1.02 http://www.aps.org/meet/DPP01/baps/tocC.html

11. E. Paller, J. Scharer, K. Akhtar, K. Kelly and G. Ding, "Radiofrequency Initiation and Radiofrequency Sustainment of Laser Initiated Seeded High Pressure Plasmas" Institute of Electrical and Electronics Engineers (IEEE) International Conference on Plasma Science, Conference Records-Abstracts. Volume 01CH37255, O2G5 abstract #0596. June 17-22, 2001. Las Vegas, Nevada.

http://ktechw3.ktech.com/~ppps/TechTopic/TechnicalTopics.html

12. K. Kelly, J. Scharer, E. Paller, "Laser Ionization and Radiofrequency Sustainment of High-Pressure Seeded Plasmas" Institute of Electrical and Electronics Engineers (IEEE) International Conference on Plasma Science, Conference Records-Abstracts. Volume 01CH37255, O2G6 abstract #0597. June17-22, 2001, Las Vegas, Nevada. . http://ktechw3.ktech.com/~ppps/TechTopic/TechnicalTopics.html

13. E.. Paller, J. Scharer, R. Cao, K. Kelly, "Air Constituent Plasmas Produced by a Radiofrequency Plasma Source" Institute of Electrical and Electronics Engineers (IEEE) International Conference on Plasma Science, Conference Records-Abstracts. Volume 01CH37255, P3B06, abstract #0598. June 17-22, 2001. Las Vegas, Nevada http://ktechw3.ktech.com/~ppps/TechTopic/TechnicalTopics.html

14. E. Paller, J. Scharer, K. Akhtar, K. Kelly and G. Ding, "Radiofrequency Initiation and Radiofrequency Sustainment of Laser Initiated Seeded High Pressure Plasmas" pp 526-529, Radio Frequency Power in Plasmas, 14th topical conference, AIP Conference Proceedings-595, Oxnard, CA May 2001. http://ojps.aip.org/proceedings/plasma_phys.jsp.

15. J. Scharer, A. Degeling, G. Borg, R. Boswell, E. Paller, R. Cao, B. White and R. Sund, "Optical Measurements of Fast Electron Effects in a Helicon Plasma" pp 522-525, Radio Frequency Power in Plasmas, 14th topical conference, AIP Conference Proceedings-595, Oxnard, CA, May 2001; Editor, Dr. T. K. Mau, my first Ph. D. student. http://ojps.aip.org/proceedings/plasma_phys.jsp

16. J.Scharer, A. Degeling, G. Borg, R. Boswell, "Optical and Magnetic Probe Measurements and Analysis for a Helicon Plasma Source" Bulletin of the American Physical Society, Division of Plasma Physics Meetings, Volume 46, No. 8, October 2001, page 31. BM1.008 http://www.aps.org/meet/DPP01/baps/tocB.html

17. A. Degeling, J. Scharer, R. Boswell, "Evidence of Electron Trapping in a Helicon Discharge," The IEEE International Conference and Plasma Science, New Orleans, June 4-7, Conf. Record 5B03, 226 (2000).

18. J. Scharer, R. Cao, H. Gui, K. Kelly, E. Paller, R. Sund, "Laser Initiation and Radiofrequency Sustainment of Seeded Air Plasma," The IEEE International Conference and Plasma Science, New Orleans, June 4-7, Conf. Record 1A07, 84 (2000).

19. G. Ding, J. Scharer, R. Cao, K. Kelly, "Diagnostic and Analysis of a Laser-produced Organic Vapor Plasma," The IEEE International Conference and Plasma Science, New Orleans, June 4-7, Conf. Record 1P27, 112 (2000).

20. K. Kelly, J. Scharer, G. Ding, E. Paller, R. Cao, "A Laser-Produced Plasma Sustained by a Radiofrequency Source," The IEEE International conference and Plasma Science, New Orleans, June 4-7, Conf. Record 1P28, 113 (2000)

21. E.S. Paller, J. E. Scharer, K. L Kelly, G. Ding, "Argon and Air Mixture Plasmas Produced by a Radiofrequency Plasma Source, "," The IEEE International Conference and Plasma Science, New Orleans, June 4-7, Conf. Record 1P29, 113 (2000).

22. K. Kelly, J. Scharer, M. Laroussi, R. Block, K. Schoenbach, "Measuring Electron Densities in Highly Collisional Plasmas Using a 110 GHz Interferometer," The IEEE International Conference and Plasma Science, New Orleans, June 4-7, Conf.Record 2P26, 147 (2000).

23. K. L. Kelly, J.E. Scharer, E. Paller, H. Gui, R Cao, "Radiofrequency Sustainment of a Laser-Produced Plasma," The IEEE International Conference and Plasma Science, New Orleans, June 4-7, Conf. Record 5B10, 229 (2000).

24. J. Scharer, E. Paller, R. Cao, "Evidence of Fast Electron Effects in a Helicon Discharge," Bull. Am. Phys. Soc. 44, 131 (2000) Quebec City, Oct 23-27.

25. K. Kelly, J. Scharer, R. Cao, G. Ding, E. Paller, "Laser Initiation and Radiofrequency Sustainment of Seeded Air Plasmas," Bull. Am. Phys. Soc. 44, 131 (2000) Quebec City, Oct 23-27.

XIII. Grant Modalities:

During the grant period, (May 2000 - May 2003), the participants carrying out the research were as follows:

1. John E. Scharer, Professor

2. Kamran Akhtar, Postdoctoral Researcher

3. Shane Tysk, Graduate Student

5. Ben White, Graduate Student

6. Mark Denning, Graduate Student

7. Guowen Ding, Graduate Student

8. Kurt L. Kelly, Graduate Student

9. Eric S. Paller, Graduate Student

10. Enny Khoe, (Undergraduate Researcher)

XIV. Students Graduated: (2000-2003)

1. Guowen Ding, Ph.D. 2001, Employed at Applied Materials, RF plasma processing.

2. Kurt L. Kelly, Ph.D., 2002, Employed at MIT Lincoln Laboratory, Laser measurements in atmospheric turbulence.

3. Eric S. Paller, MS Thesis, 2002, Employed at Titan Industries, Antennas.

4. Ben White, MS Thesis, 2002, Employed at Motorola, Antennas and Communications.